

Decoding $Z_c(4430)$ and $Z_c(4200)$: The role of P -wave charmed mesons

Jian-Bo Cheng^{1,2} *, Zi-Yang Lin² †, Jun-Zhang Wang³ ‡ and Shi-Lin Zhu² §

¹College of Science, China University of Petroleum, Qingdao, Shandong 266580, China

²School of Physics and Center of High Energy Physics, Peking University, Beijing 100871, China

³Department of Physics and Chongqing Key Laboratory for Strongly Coupled Physics, Chongqing University, Chongqing 401331, China

In this work, we perform a systematic investigation of the hidden-charm tetraquark states with $I^G(J^{PC}) = 1^+(1^{+-})$ within the hadronic molecular picture, placing particular emphasis on systems composed of an S -wave (D, D^*) meson and a P -wave ($D_0^*(2300), D_1(2430), D_1(2420), D_2^*(2460)$) meson. Adopting the One-Boson Exchange potential, we solve the Schrödinger equation in momentum space via the Complex Scaling Method. A crucial feature of our approach is the rigorous treatment of the unstable nature of the P -wave constituents by incorporating three-body decay effects arising from self-energy corrections and the static limit approximation. Our results demonstrate that these three-body dynamics play a crucial role in determining the pole positions, specifically in reproducing the large decay widths observed experimentally. We identify several broad resonances in the $D^* \bar{D}_1(2420)$ and $D^* \bar{D}_2^*(2460)$ systems as candidates for the $Z_c(4430)$, while the significantly broader resonances in the $D \bar{D}_0^*(2300)$ and $D \bar{D}_1(2430)$ sectors are suggested as candidates for the $Z_c(4200)$. Focusing on the $D^* \bar{D}_2^*(2460)$ assignment as a specific case study, we further analyze the line shape of the $Z_c(4430)$ candidate using a Flatté-like parametrization with energy-dependent self-energy terms, providing predictions for its open-charm decay modes to guide future experimental searches.

I. INTRODUCTION

The observation of the $X(3872)$ by the Belle Collaboration in 2003 [1] marked the dawn of a new era in hadron physics, revealing a rich spectrum of exotic candidates that defy the conventional $c\bar{c}$ quark model. Following this, the discovery of the charged charmonium-like states, such as the $Z_c(3900)$ and $Z_c(4020)$ by the BESIII and Belle Collaborations [2–4], provided unambiguous evidence for the existence of multiquark states with a minimal content of $c\bar{c}ud\bar{d}$. More recently, the LHCb Collaboration reported the T_{cc}^+ [5, 6], a double-charm tetraquark candidate lying just below the $D^{*+}D^0$ threshold, which further enriched the landscape of exotic hadrons. For a broader perspective, comprehensive reviews published in recent years offer further insights into this field [7–20].

Given that the $Z_c(3900)$ and $Z_c(4020)$ lie remarkably close to the $D\bar{D}^*$ and $D^*\bar{D}^*$ thresholds, respectively, a leading theoretical interpretation is that they are candidates for S -wave hadronic molecules [21–36], although their exact nature continues to be a subject of active research. While the low-lying S -wave molecular sector is relatively well-established, the nature of the higher-mass excited states remains an intriguing topic. A very recent experimental study [37] reported updated observations of the $Z_c(4430)$, determining its mass and width as:

$$M = 4.452 \pm 0.016^{+0.055}_{-0.033} \text{ GeV}, \quad \Gamma = 0.174 \pm 0.019^{+0.083}_{-0.020} \text{ GeV}. \quad (1)$$

This study also analyzed the detailed structure and corresponding decay modes of the state. Historically, the $Z_c(4430)$ has been a focal point of exotic hadron research for over a decade. It was first observed by the Belle Collaboration in the $\psi(2S)\pi^+$ invariant mass spectrum [38] and subsequently confirmed by LHCb with high significance [39], which determined its preferred quantum numbers to be $J^P = 1^+$. Unlike the $Z_c(3900)$, the $Z_c(4430)$ is characterized by a significantly broader width and a mass lying far above the ground-state open-charm thresholds (such as $D\bar{D}^*$), complicating its theoretical interpretation.

The prevailing theoretical perspective interprets the $Z_c(4430)$ as a hadronic molecule composed of two charmed mesons. In early works [40, 41], the authors explored the possibility of $Z_c(4430)$ as an S -wave $D^* \bar{D}_1(2430)/D^* \bar{D}_1(2420)$ molecular state. Utilizing the One-Boson Exchange (OBE) model, Refs. [42, 43] further investigated the P -wave $D^* \bar{D}_1(2420)$ molecular scenario. Ma et al. [44] studied the decay processes considering both the S -wave $\bar{D}D^*(2600)$ and the P -wave excited $D^* \bar{D}_2^*(2460)$ molecular configurations. Furthermore, assuming a $\bar{D}D^*(2600)$ structure, Liu et al. [45] analyzed the decay mechanisms, specifically comparing the $\psi(2S)\pi$ and $J/\psi\pi$ channels. The production mechanisms of this state have also been investigated in Refs. [46, 47]. Beyond the molecular picture, alternative explanations have been proposed, including the compact tetraquark structure [48–56], triangle singularities [57, 58], and threshold effects [59].

A critical puzzle that motivates the present work is the anomalous ratio of the branching fractions for $Z_c(4430)$ (and the related structure). Experimentally, these states exhibit a strong preference for decaying into $\psi(2S)\pi$ over $J/\psi\pi$, with a ratio $R \approx 10$. This behavior stands in

* jbcheng@pku.edu.cn

† lzy_15@pku.edu.cn

‡ wangjzh@cqu.edu.cn

§ zhusl@pku.edu.cn

sharp contrast to the ground state $Z_c(3900)$, where the $J/\psi\pi$ is the discovery mode and the $\psi(2S)\pi$ mode is suppressed. This observation strongly suggests that these high-mass states possess an internal structure different from the S -wave molecules; specifically, they are likely composed of excited P -wave charmed mesons. The radially excited nature or the spatial extension due to the P -wave centrifugal barrier would naturally facilitate the overlap with the $\psi(2S)$ wave function, thereby explaining the enhanced decay width.

However, investigating molecular states involving P -wave constituents—such as the scalar $D_0^*(2300)$ (denoted as D_0^*), the axial-vector $D_1(2420)/D_1(2430)$ (denoted as D_1/D_1'), or the tensor $D_2^*(2460)$ (denoted as D_2^*)—requires moving beyond standard approximations that treat constituents as stable particles. Such simplified approaches neglect the significant decay widths of these mesons (primarily into $D^{(*)}\pi$) and the resulting three-body dynamics. Given their inherent instability, the molecular systems $D^*\bar{D}'_1$, $D^*\bar{D}_1$, and $D^*\bar{D}_2^*$ are inevitably coupled to three-body continua. As demonstrated in previous studies on the $D\bar{D}^*$ system [60, 61], the three-body decay effects arising from the static limit correction (recoil effect) and self-energy diagrams can significantly shift the pole positions and, in particular, drastically amplify the widths. Given that the phase space and energy transfer for the decays of P -wave charmed mesons are much larger than those for D^* , these effects are expected to be even more pronounced in the present systems. Therefore, a systematic study is required. In this work, we investigate the $1^+(1^{+-})$ Z_c systems composed of an S -wave and a P -wave charmed meson, explicitly incorporating the open-charm three-body decay effects and analyzing the corresponding line shapes.

The paper is organized as follows. In Sec. II, we introduce the theoretical framework, including the coupled-channel formalism and the complex scaling method (CSM) incorporating width effects for unstable particles. In Sec. III, we construct the effective Lagrangians based on heavy quark and chiral symmetries, estimate the coupling constants, and derive the OBE potentials. In Sec. IV, we present the numerical results, analyzing the pole positions under the instantaneous approximation, static limit correction, and self-energy contributions. We also discuss the identification of the $Z_c(4430)$ and $Z_c(4200)$ candidates and analyze the line shape of the latter. Finally, a summary is given in Sec. V.

II. FRAMEWORK

In this work, we investigate the nature of $Z_c(4430)$ and $Z_c(4200)$ by considering interactions involving the (D, D^*) , (D_0^*, D_1') , and (D_1, D_2^*) doublets with spin-parity $(0^-, 1^-)$, $(0^+, 1^+)$, and $(1^+, 2^+)$, respectively. To perform a systematic analysis of the $I^G(J^{PC}) = 1^+(1^{+-})$ hidden-charm sector, coupled-channel effects are explicitly included. This leads to 10 subsystems with 15

distinct channels, see Table II. The first seven sectors are single-channel systems. The 8th (D^*D_1') and 9th (D^*D_1) sectors involve three partial waves (1P_1 , 3P_1 , 5P_1), whereas the 10th sector ($D^*D_2^*$) involves two (3P_1 , 5P_1).

In previous works [60, 62], we investigated double- and hidden-charm tetraquarks using the CSM. We found that the unstable nature of the D^*/\bar{D}^* mesons contributes an imaginary part to the OPE potential. This phenomenon is referred to as the three-body decay effect in our framework. Consequently, the $DD^*({}^3S_1)$ bound state, which corresponds to the T_{cc}^+ , acquires a small width. In this article, we assume that similar interactions exist in the OPE terms of the $D\bar{D}^* \leftrightarrow D_0^*\bar{D}$, $D^*\bar{D}'_1 \leftrightarrow D_1'\bar{D}^*$, $D\bar{D}_2^* \leftrightarrow D_2^*\bar{D}$, $D^*\bar{D}_1 \leftrightarrow D_1\bar{D}^*$, and $D^*\bar{D}_2^* \leftrightarrow D_2\bar{D}^*$ channels.

For molecular states composed of these unstable particles, we must also consider the three-body decay effects arising from the self-energy terms of the unstable components, specifically D_0^* , D_1' , D_1 , and D_2^* . Based on our previous analysis [62], the contribution of these self-energy terms to the total width is expected to be comparable to, or even larger than, that of the three-body effects in the OPE potential. Therefore, we will also investigate the impact of these self-energy effects on the Z_c system.

$I^G(J^{PC})$	$1^-(0^{-+})$	$0^+(0^{-+})$	$0^+(0^{++})$	$1^+(1^{--})$	$0^-(1^{--})$
Meson	π	η	σ	ρ	ω
M (MeV)	138.04	547.86	500	775.26	782.66
J^P	0^-	1^-	0^+	1^+	
Meson	D	D^*	D_0^*	D_1'	
M (MeV)	1867.25	2008.55	2343 ± 10	2412 ± 9	
Γ (MeV)	-	-	229 ± 16	314 ± 29	
J^P	1^+	2^+			
Meson	D_1	D_2^*			
M (MeV)	2422.1 ± 0.6	2461.1 ± 0.7			
Γ (MeV)	31.3 ± 1.9	47.3 ± 0.8			

TABLE I. The average masses (in units of MeV) of the charmed and light mesons, which are taken from Ref. [63].

A. A brief discussion on the CSM

In this work, we adopt the complex scaling method (CSM), originally proposed by Aguilar, Balslev, and Combes in the 1970s [64, 65], along with the improved complex scaling method [66], to investigate bound states, resonances, and virtual states in momentum space. The transformations of the coordinate r and momentum k in the CSM are defined as:

$$U(\theta)r = re^{i\theta}, \quad U(\theta)k = ke^{-i\theta}. \quad (2)$$

Following the complex scaling operation, the

Channel	1	2	3	4	5	6	7	
System	$\{D\bar{D}^*\}(^3S_1)$	$D^*\bar{D}^*(^3S_1)$	$\{D\bar{D}_0^*\}(^1P_1)$	$\{D\bar{D}'_1\}(^3P_1)$	$\{D\bar{D}_1\}(^3P_1)$	$[D\bar{D}_2^*](^5P_1)$	$[D^*\bar{D}_0^*](^3P_1)$	
Channel	8	9	10	11	12	13	14	15
System	$[D^*\bar{D}'_1](^1P_1)$	$\{D^*\bar{D}'_1\}(^3P_1)$	$[D^*\bar{D}'_1](^5P_1)$	$[D^*\bar{D}_1](^1P_1)$	$\{D^*\bar{D}_1\}(^3P_1)$	$[D^*\bar{D}_1](^5P_1)$	$\{D^*\bar{D}_2\}(^3P_1)$	$[D^*\bar{D}_2](^5P_1)$

TABLE II. The channels of the hidden-charm tetraquark systems with $I^G(J^{PC}) = 1^+(1^{+-})$. We adopt the following shorthand notations for simplicity: $[A, \bar{B}] = \frac{1}{\sqrt{2}}(A\bar{B} - B\bar{A})$ and $\{A, \bar{B}\} = \frac{1}{\sqrt{2}}(A\bar{B} + B\bar{A})$.

Schrödinger equation

$$\frac{p^2}{2m}\phi_l(p) + \int \frac{p'^2 dp'}{(2\pi)^3} V_{l,l'}(p, p') \phi_{l'}(p') = E\phi_l(p), \quad (3)$$

in momentum space transforms into

$$\frac{p^2 e^{-2i\theta}}{2m} \tilde{\phi}_l(p) + \int \frac{p'^2 e^{-3i\theta} dp'}{(2\pi)^3} V_{l,l'}(pe^{-i\theta}, p'e^{-i\theta}) \tilde{\phi}_{l'}(p') = E\tilde{\phi}_l(p), \quad (4)$$

subject to the normalization condition [67]

$$\frac{e^{-3i\theta}}{(2\pi)^3} \int_0^\infty \tilde{\phi}_l(p)^2 p^2 dp = 1, \quad (5)$$

where l and l' denote the orbital angular momenta, and p represents the relative momentum in the center-of-mass frame. The potential $V_{l,l'}$, obtained after partial wave decomposition, is expressed as

$$\begin{aligned} V_{l,l'} = & \int d\Omega' \int d\Omega \sum_{m_{l'}=-l'}^{l'} \langle l', m_{l'}; s, m_j - m_{l'} | j, m_j \rangle \\ & \times \sum_{m_l=-l}^l \langle l, m_l; s, m_j - m_l | j, m_j \rangle \mathcal{Y}_{l',m_{l'}}^*(\theta', \phi') \\ & \times \mathcal{Y}_{l,m_l}(\theta, \phi) \langle s, m_j - m_{l'} | \mathcal{V} | s, m_j - m_l \rangle, \end{aligned} \quad (6)$$

Here, s and j represent the total spin and total angular momentum of the system, respectively, and m_l is the corresponding magnetic quantum number. $\mathcal{Y}_{l,m_l}(\theta, \phi)$ denotes the spherical harmonics associated with the angular coordinates θ and ϕ . The potential operator \mathcal{V} acts on the states $|s, m_j - m_{l'}\rangle$ and $|s, m_j - m_l\rangle$.

We introduce a non-local monopole form factor to suppress potential contributions in the high-momentum region, defined as

$$F(p'^2, p^2) = \frac{\Lambda^2}{\Lambda^2 + p'^2} \frac{\Lambda^2}{\Lambda^2 + p^2}, \quad (7)$$

where Λ represents the cutoff parameter.

In the present work, we treat the D and D^* mesons as stable particles, whereas the broad states D_0^* , D'_1 , D_1 , and D_2^* are considered unstable. To incorporate the effects of their decays, we modify the complex-scaled Schrödinger equation in momentum space as follows:

$$\left(\frac{p^2 e^{-2i\theta}}{2m} - \frac{i}{2} \Gamma(E, pe^{-i\theta}) \right) \tilde{\phi}_l(p)$$

$$+ \int \frac{p'^2 e^{-3i\theta} dp'}{(2\pi)^3} V_{l,l'}(pe^{-i\theta}, p'e^{-i\theta}) \tilde{\phi}_{l'}(p') = E\tilde{\phi}_l(p), \quad (8)$$

where $\Gamma(E, pe^{-i\theta})$ represents the width of the unstable meson following the complex scaling transformation.

Taking the $D\bar{D}_0^*$ system as an example, the expression for the width prior to complex scaling is given by

$$\Gamma_{D_0^*}(E, p) = \frac{3}{2} \frac{f''^2}{2\pi f_\pi^2} \frac{m_D}{m_{D_0^*}} k_\pi E_\pi^2. \quad (9)$$

The factor of 3/2 accounts for isospin, corresponding to the sum of the charged (π^\pm , factor 1) and neutral (π^0 , factor 1/2) channels. Here, k_π and E_π denote the momentum and energy of the final-state pion, respectively defined as

$$\begin{aligned} k_\pi &= \frac{1}{2E_{D_0^*}} \lambda^{1/2}(E_{D_0^*}^2, m_D^2, m_\pi^2), \\ E_{D_0^*} &= [(E - \sqrt{p^2 + m_D^2})^2 - p^2]^{1/2}, \\ \lambda(a, b, c) &= a^2 + b^2 + c^2 - 2ab - 2bc - 2ac, \end{aligned} \quad (10)$$

where $E_{D_0^*}$ represents the effective invariant mass of the D_0^* component when the total energy of the system is E and the spectator D meson is on-shell.

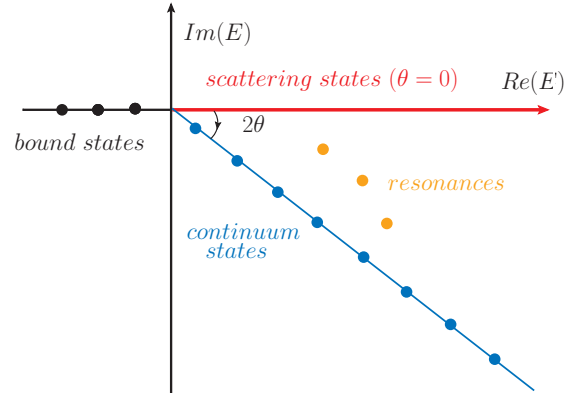


FIG. 1. The eigenvalue distribution of the complex scaled Schrödinger equation for the two-body systems.

III. LAGRANGIANS AND POTENTIALS

A. Lagrangians

We adopt the OBE potential to describe the interactions between two heavy mesons. The effective Lagrangians are constructed based on heavy quark symmetry and chiral symmetry. The explicit expressions are given by

$$\begin{aligned}\mathcal{L}_{\pi/\eta} = & g\langle H_b \mathbb{A}_{ba} \gamma_5 \bar{H}_a \rangle + g'\langle S_b \mathbb{A}_{ba} \gamma_5 \bar{S}_a \rangle + g''\langle T_b^\mu \mathbb{A}_{ba} \gamma_5 \bar{T}_a^\mu \rangle \\ & + f''\langle S_b \mathbb{A}_{ba} \gamma_5 \bar{H}_a \rangle + f'\langle T_b^\mu A_{\mu ba} \gamma_5 \bar{S}_a \rangle \\ & + \frac{i}{\Lambda_\chi} \langle T_b^\mu (h_1 D_\mu \mathbb{A} + h_2 \not{D} A_\mu)_{ba} \gamma_5 \bar{H}_a \rangle + \text{H.c.},\end{aligned}\quad (11)$$

$$\begin{aligned}\mathcal{L}_{\rho/\omega} = & i\beta\langle H_b v^\mu (V_\mu - \rho_\mu)_{ba} \bar{H}_a \rangle + i\lambda\langle H_b \sigma^{\mu\nu} F_{\mu\nu}(\rho)_{ba} \bar{H}_a \rangle \\ & + i\beta_1\langle S_b v^\mu (V_\mu - \rho_\mu)_{ba} \bar{S}_a \rangle + i\lambda_1\langle S_b \sigma^{\mu\nu} F_{\mu\nu}(\rho)_{ba} \bar{S}_a \rangle \\ & + i\beta_2\langle T_b^\mu v^\nu (V_\nu - \rho_\nu)_{ba} \bar{T}_{\mu a} \rangle + i\lambda_2\langle T_b^\mu \sigma^{\alpha\beta} F_{\alpha\beta}(\rho)_{ba} \bar{T}_{\mu a} \rangle \\ & + i\zeta\langle H_b \gamma^\mu (V_\mu - \rho_\mu)_{ba} \bar{S}_a \rangle + i\mu\langle H_b \sigma^{\mu\nu} F_{\mu\nu}(\rho)_{ba} \bar{S}_a \rangle \\ & + i\zeta_1\langle T_b^\mu (V_\mu - \rho_\mu)_{ba} \bar{H}_a \rangle + \mu_1\langle T_b^\mu \gamma^\nu F_{\mu\nu}(\rho)_{ba} \bar{H}_a \rangle \\ & + \mu_2\langle T_b^\mu \gamma^\nu F_{\mu\nu}(\rho)_{ba} \bar{S}_a \rangle + \text{H.c.},\end{aligned}\quad (12)$$

$$\begin{aligned}\mathcal{L}_\sigma = & g_\sigma\langle H_a \sigma \bar{H}_a \rangle + g'_\sigma\langle S_a \sigma \bar{S}_a \rangle + g''_\sigma\langle T_a^\mu \sigma \bar{T}_{a\mu} \rangle \\ & + \frac{ih_\sigma}{f_\pi}\langle S_a (\partial_\mu \sigma) \gamma^\mu \bar{H}_a \rangle + \frac{ih'_\sigma}{f_\pi}\langle T_a^\mu (\partial_\mu \sigma) \bar{H}_a \rangle + \text{H.c.}\end{aligned}\quad (13)$$

Here, the superfields H_a , S_a , and T_a^μ represent the heavy meson doublets with spin-parity content $(0^-, 1^-)$, $(0^+, 1^+)$, and $(1^+, 2^+)$, respectively. Their explicit expressions are given by

$$H_a^{(Q)} = \frac{1+\not{\psi}}{2} [P_a^{*\mu} \gamma_\mu - P_a \gamma_5], \quad (14)$$

$$S_a^{(Q)} = \frac{1+\not{\psi}}{2} [P_{1a}^\mu \gamma_\mu \gamma_5 - P_{0a}^*], \quad (15)$$

$$T_a^\mu = \frac{1+\not{\psi}}{2} \left\{ P_{2a}^{*\mu\nu} \gamma_\nu - \sqrt{\frac{3}{2}} P_{1a}^\nu \gamma_5 \left[g_\nu^\mu - \frac{1}{3} \gamma_\nu (\gamma^\mu - v^\mu) \right] \right\}, \quad (16)$$

where a denotes the flavor index, and the multiplet components are defined as $P_a^{(*)} = (D^{(*)0}, D^{(*)+}, D_s^{(*)+})$. Similarly, the components of the excited doublets are defined as $P_{0a}^* = (D_0^{*0}, D_0^{*+}, D_{s0}^{*+})$, $P_{1a}' = (D_1'^0, D_1'^+, D_{s1}^+)$, $P_{1a} = (D_1^0, D_1^+, D_{s1}^+)$, and $P_{2a}^* = (D_2^{*0}, D_2^{*+}, D_{s2}^{*+})$.

The fields involving light mesons are defined as follows:

$$\mathbb{A}_\mu = \frac{i}{2} [\xi^\dagger (\partial_\mu \xi) + (\partial_\mu \xi) \xi^\dagger], \quad (17)$$

$$V_\mu = \frac{i}{2} [\xi^\dagger (\partial_\mu \xi) - (\partial_\mu \xi) \xi^\dagger], \quad (18)$$

with $\xi = \exp(i\mathcal{M}/f_\pi)$, where the pseudoscalar meson matrix is

$$\mathcal{M} = \begin{pmatrix} \frac{\pi^0}{\sqrt{2}} + \frac{\eta}{\sqrt{6}} & \pi^+ & K^+ \\ \pi^- & -\frac{\pi^0}{\sqrt{2}} + \frac{\eta}{\sqrt{6}} & K^0 \\ K^- & \bar{K}^0 & -\frac{2}{\sqrt{6}}\eta \end{pmatrix}. \quad (19)$$

The vector meson field is given by $\rho^\mu = i\frac{g_V}{\sqrt{2}}\hat{\rho}^\mu$, with

$$\hat{\rho}^\mu = \begin{pmatrix} \frac{\rho^0}{\sqrt{2}} + \frac{\omega}{\sqrt{2}} & \rho^+ & K^{*+} \\ \rho^- & -\frac{\rho^0}{\sqrt{2}} + \frac{\omega}{\sqrt{2}} & K^{*0} \\ K^{*-} & \bar{K}^{*0} & \phi \end{pmatrix}^\mu. \quad (20)$$

Here, the pion decay constant is taken as $f_\pi = 132$ MeV. The remaining coupling constants are determined via the quark model. The specific values adopted in our calculation are summarized in Table III. Detailed discussions regarding their extraction and the relevant coupling relations are provided in Appendix VI B.

TABLE III. Coupling constants used in the calculation.

g	g'	g''	f'	f''	$\frac{h_1+h_2}{\Lambda_\chi}$
-0.59	0.25	0.75	-0.87	0.53	1.03 GeV $^{-1}$
β	β_1	β_2	λ	λ_1	λ_2
0.9	-0.9	-0.9	0.56 GeV $^{-1}$	0.19 GeV $^{-1}$	-0.56 GeV $^{-1}$
g_V	ζ	ζ_1	μ	μ_1	μ_2
5.8	0.81	1.40	-1.00 GeV $^{-1}$	-1.74 GeV $^{-1}$	-1.29 GeV $^{-1}$
g_σ	g'_σ	g''_σ	h_σ	h'_σ	
2.73	-2.73	-2.73	0.48		-0.48

The explicit expressions for the expanded Lagrangians describing the interactions between heavy flavor mesons and light mesons ($\pi, \sigma, \rho/\omega$) are detailed in Appendix VIA.

B. Potential

The explicit expressions for the OBE potentials in the diagonal sectors are presented in momentum space in Appendix VI C. As an illustrative example, consider the $\{D\bar{D}^*\}(^3S_1)$ channel:

$$\begin{aligned}V(D\bar{D}^* \rightarrow D\bar{D}^*) = & \delta_C \frac{g^2}{2f_\pi^2} (\vec{q} \cdot \vec{\epsilon}_3^\dagger) (\vec{q} \cdot \vec{\epsilon}_1) \\ & \times \left(\frac{\vec{\tau}_1 \cdot \vec{\tau}_2}{q^2 - m_\pi^2} - \frac{1/3}{q^2 - m_\eta^2} \right) + g_\sigma^2 \frac{\vec{\epsilon}_4^\dagger \cdot \vec{\epsilon}_2}{q^2 - m_\sigma^2} \\ & + g_V^2 \left\{ -\frac{1}{4} \beta^2 (\vec{\epsilon}_4^\dagger \cdot \vec{\epsilon}_2) - \delta_C \lambda^2 \left[\vec{q}^2 (\vec{\epsilon}_3^\dagger \cdot \vec{\epsilon}_2) \right. \right. \\ & \left. \left. - (\vec{q} \cdot \vec{\epsilon}_3^\dagger) (\vec{q} \cdot \vec{\epsilon}_2) \right] \right\} \left(\frac{\vec{\tau}_1 \cdot \vec{\tau}_2}{q^2 - m_\rho^2} - \frac{1}{q^2 - m_\omega^2} \right).\end{aligned}\quad (21)$$

where $\vec{\epsilon}$ denotes the polarization vector of the D^*/\bar{D}^* meson. The indices 1, 2, 3, 4 label the particles, such that particles 1 and 3 (2 and 4) share a vertex. δ_C represents a phase factor arising from the cross-channel diagrams, determined by the symmetry of the final state flavor configuration: $\delta_C = 1$ for $\{AB\}$ and $\delta_C = -1$ for $[A\bar{B}]$. Obviously, $\delta_C = 1$ for the process $\{D\bar{D}^*\}(^3S_1) \rightarrow \{D\bar{D}^*\}(^3S_1)$.

As discussed in Refs. [60, 61, 68], in the OPE cross-channel diagrams, the condition $|q^0| \approx m_{D^*} - m_D > m_\pi$ can induce a three-body mediated decay effect. This effect significantly influences the imaginary part of the pole near the threshold. It becomes particularly pronounced for the $D^{(*)}\bar{D}_0^*$, $D^{(*)}\bar{D}_1'$, $D^{(*)}\bar{D}_1$, and $D^{(*)}\bar{D}_2^*$ cases, where the energy transfer $|q^0|$ is much larger than that in the $D\bar{D}^*$ case.

Assuming the final state is at rest, the transferred energy carried by the exchanged light meson is given by

$$q^0 = \frac{m_1^2 - m_2^2 - m_3^2 + m_4^2}{2(m_3 + m_4)}, \quad (22)$$

where indices 1, 2 (3, 4) correspond to the initial (final) particles. In the diagonal sector, this static limit approximation implies zero recoil correction, as the initial and final kinetic energies both vanish. We list the q^0 values for the direct (q_{0D}) and cross (q_{0C}) diagrams in the diagonal channels in Table IV. It is evident that $q_{0D} = 0$ for direct diagrams, while $q_{0C} = m_1 - m_2$. When $|q^0| > m_\pi$, the three-body decay effect emerges, potentially affecting the particle widths significantly.

System	$D\bar{D}^*$	$D^*\bar{D}^*$	$D\bar{D}_0^*$	$D\bar{D}_1'$	$D\bar{D}_1$
q_{0D}	0	0	0	0	0
q_{0C}	-141	0	-476	-545	-555
System	$D\bar{D}_2^*$	$D^*\bar{D}_0^*$	$D^*\bar{D}_1'$	$D^*\bar{D}_1$	$D^*\bar{D}_2^*$
q_{0D}	0	0	0	0	0
q_{0C}	-594	-334	-403	-414	-453

TABLE IV. The transferred energy values q_{0D} and q_{0C} (in units of MeV) for the diagonal channels calculated in the static limit. Note that q_{0D} vanishes for all diagonal channels in this approximation.

In the isovector molecular case, it is straightforward to observe that the One-Vector-Exchange (OVE) term is proportional to $(1/(q^2 - m_\rho^2) - 1/(q^2 - m_\omega^2))$, where the two terms largely cancel each other. Consequently, the OVE contribution is negligible. Similarly, the η exchange term is suppressed to about 1/3 of the pion strength. Therefore, the dominant interactions arise from the OPE and One-Sigma-Exchange (OSE) potentials. At this stage, the determination of g_σ becomes crucial. In Ref. [69], the authors utilized the specific exotic state $Z_c(3900)$ as input to constrain g_σ . In the present study, as detailed in the Appendix VI B, we adopt the chiral quark model, setting $g_\sigma = 2.73$.

The partial-wave projected potentials for the diagonal sectors are also provided in Appendix VI C. Notably, for the spin-mixing transition $(^1P_1) \rightarrow (^3P_1)$ in the D^*D_1' sector, the potential vanishes ($V_{89} = 0$). However, this is not the case for the $(^1P_1) \rightarrow (^5P_1)$ transition. This phenomenon was also observed in a recent study of the \bar{D}^*K^* system [70], where the potential for the $(^{1,5}P_1) \rightarrow (^3P_1)$ process was found to be zero. The underlying reason is that both \bar{D}^* and K^* (or our D^* and D_1') carry spin 1,

and their spin wave functions possess specific symmetry properties under particle exchange. The $(^1P_1)$ and $(^5P_1)$ states share the same spin symmetry, whereas the $(^3P_1)$ state has opposite symmetry. Consequently, the matrix element of the potential between these states vanishes:

$$\langle ^3P_1 | \hat{V} | ^1, ^5P_1 \rangle \equiv 0. \quad (23)$$

Finally, we plot the diagonal sector potentials in Fig. 2, and verify that a similar vanishing potential occurs in the D^*D_1' and D^*D_1 sectors.

IV. NUMERICAL RESULTS

In our previous studies [62], we interpreted the T_{cc}^+ , $X(3872)$, $G(3900)$, and $Z_c(3900)$ as $DD^*/D\bar{D}^*$ molecules with quantum numbers $0(1^+)$, $0^+(1^{++})$, $0^-(1^-)$, and $1^+(1^{+-})$, respectively. In the present work, however, we introduce a different coupling constant $g_\sigma = 2.73$ (compared to $g_\sigma = 0.76$ in Ref. [62]) based on the chiral quark model estimation. Since this larger coupling significantly enhances the attractive strength of the σ exchange potential, the cutoff Λ must be adjusted accordingly to maintain physical consistency.

Under the instantaneous approximation ($q^0 = 0$), we reconsider the $DD^*/D\bar{D}^*$ molecules and set the cutoff to $\Lambda = 0.5$ GeV for the $g_\sigma = 0.76$ scheme, while determining $\Lambda = 0.35$ GeV for the $g_\sigma = 2.73$ scheme. The calculated results for the exotic states T_{cc}^+ , $X(3872)$, $G(3900)$, $Z_c(3900)$, and $Z_c(4020)$ under these two parameter schemes are presented in Table V. In the $g_\sigma = 2.73$ scheme, the $Z_c(3900)$ and $Z_c(4020)$ are identified as virtual states lying very close to their respective thresholds, which reflects a dominant molecular nature composed of $D^{(*)}\bar{D}^*$ components. Despite this quantitative shift, we observe that the overall conclusions remain consistent with those reported in Ref. [62].

However, the cutoff parameter determined from the DD^* system may not be suitable for the sectors involving the P -wave (D_0^*, D_1') and (D_1, D_2^*) doublets. This difference in intrinsic parity leads to a potential structure distinct from the S -wave case. Furthermore, as discussed in Appendix VI B, the momentum transfer $|\vec{q}|$ in the cross-channel diagrams is significantly higher than that in the DD^* system, suggesting that a larger cutoff Λ should be selected. Consequently, we will determine the cutoff parameter for these sectors independently.

A. The P -wave Z_c systems

We first present the results obtained under the instantaneous approximation ($q^0 = 0$), as listed in the third column of Table VI. In the single-channel systems $\{D\bar{D}_0^*\}(^1P_1)$, $\{D\bar{D}_1'\}(^3P_1)$, $\{D\bar{D}_1\}(^3P_1)$, $[D\bar{D}_2^*](^5P_1)$, and $[D^*\bar{D}_0^*](^3P_1)$, we consistently observe a similar resonance pole located below the threshold. This finding

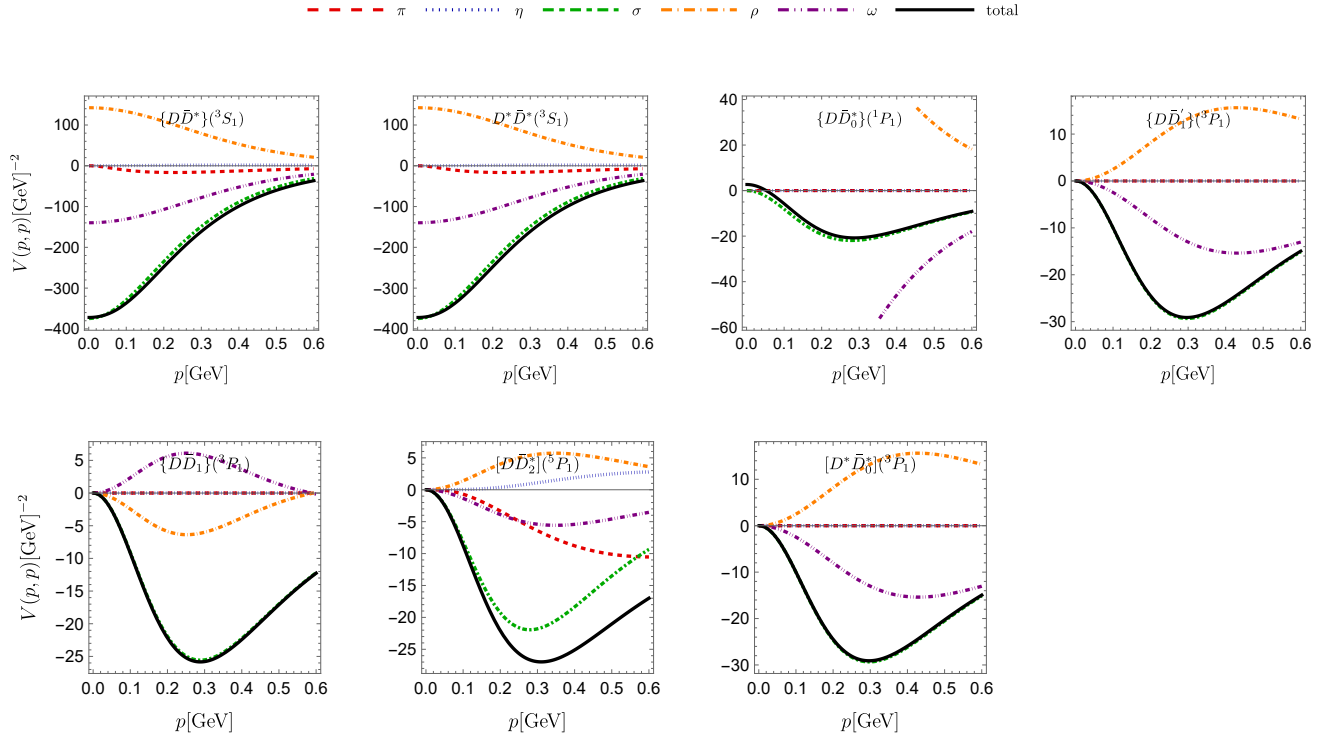


FIG. 2. The OBE potentials for the diagonal channels: $\{D\bar{D}^*\}(^3S_1)$, $D^*\bar{D}^*(^3S_1)$, $\{D\bar{D}_0^*\}(^1P_1)$, $\{D\bar{D}'_1\}(^3P_1)$, $\{D\bar{D}_1\}(^3P_1)$, $[D\bar{D}_2^*](^5P_1)$, and $[D^*\bar{D}_0^*](^3P_1)$, with quantum numbers $I^G(J^{PC}) = 1^+(1^{+-})$. The results are obtained using the instantaneous approximation ($q_0 = 0$) and a non-local regulator with cutoff $\Lambda = 0.6$ GeV.

System $I(J^P)/I^G(J^{PC})$	$DD^*(^3S_1)$	$[D\bar{D}^*](^3S_1)$	$[D\bar{D}^*](^3P_1)$	$[D\bar{D}^*](^3S_1)$	$D^*\bar{D}^*(^3S_1)$
$E(g_\sigma = 0.76, \Lambda = 500 \text{ MeV})$	$0(1^+)$	$0^+(1^{++})$	$0^-(1^{--})$	$1^+(1^{+-})$	$1^+(1^{+-})$
$E(g_\sigma = 2.73, \Lambda = 350 \text{ MeV})$	-0.57^B	-3.2^B	$-3.8 - 27.0i$	-25.8^V	-24.4^V

TABLE V. The eigenenergies (in units of MeV) relative to the corresponding thresholds: 3875.8 MeV for the first four systems and 4017.1 MeV for the fifth system. The extracted poles correspond to the molecular candidates for the exotic states T_{cc}^+ , $X(3872)$, $G(3900)$, $Z_c(3900)$, and $Z_c(4020)$, respectively. The superscripts B and V denote bound states and virtual states, respectively; otherwise, the pole represents a resonance. In both schemes, the instantaneous approximation $q^0 = 0$ is adopted.

mirrors the analysis of the $G(3900)$ as a P -wave $D\bar{D}^*$ resonance in Ref. [62], where we proposed that the centrifugal barrier inherent to P -wave systems facilitates the formation of resonant states. In contrast, for the S -wave $Z_c(3900)$ candidate, the attractive potential is deeper, favoring the formation of bound or virtual states. Due to the centrifugal barrier present in these P -wave systems, the wave function is effectively shielded from the short-range region. Consequently, the contributions from short-range interactions (such as η , ρ , and ω exchanges) are significantly reduced, rendering the system more sensitive to the medium- and long-range potentials dominated by π and σ exchanges.

An examination of the potential forms in Eq. (57),

(58), (60) reveals that the $\{D\bar{D}'_1\}(^3P_1)$, $\{D\bar{D}_1\}(^3P_1)$, and $[D^*\bar{D}_0^*](^3P_1)$ channels receive no contribution from the OPE term; their interactions are governed almost entirely by the OSE potential. Although the $\{D\bar{D}_0^*\}(^1P_1)$ channel contains an OPE term, its contribution is proportional to the transferred energy q_{0C} in the cross-diagram, which vanishes in the instantaneous approximation. The $[D\bar{D}_2^*](^5P_1)$ channel does include an OPE contribution, but as shown in Fig. 2, its magnitude is small. Therefore, considering Heavy Quark Spin Symmetry (HQSS), it is natural to observe highly similar pole positions and behaviors across these systems.

In the $D^*\bar{D}'_1$ sector, spin-mixing occurs between the $(^1P_1)$ and $(^5P_1)$ partial waves, whereas the $(^3P_1)$ chan-

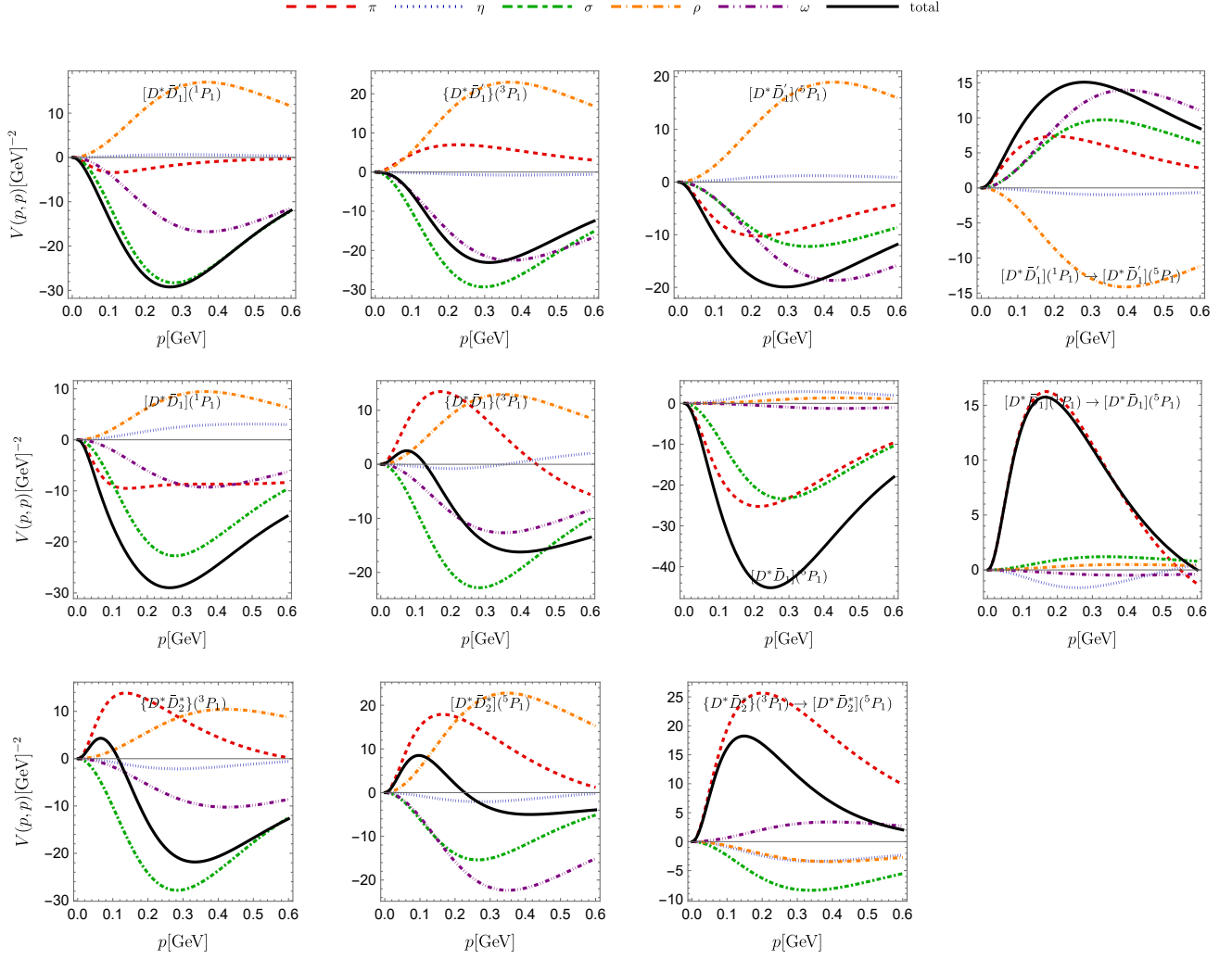


FIG. 3. The OBE potentials for the diagonal sectors of $D^*\bar{D}'_1$, $D^*\bar{D}_1$, and $D^*\bar{D}_2^*$ with quantum numbers $I^G(J^{PC}) = 1^+(1^{+-})$. The potentials for the non-vanishing spin-mixing transitions among the $(^1,^3,^5P_1)$ partial waves are also displayed. The parameters are the same as in Fig. 2.

nel remains decoupled. Evidently, the behavior of the isolated $(^3P_1)$ channel parallels that of the other single-channel systems. The coupling strength between a pole and the $(^1P_1)$ or $(^5P_1)$ channel is reflected in the residue of the T -matrix. To quantify the effective coupling constant g_Z via the residue, we introduce the relation:

$$g_Z^2 \propto \lim_{E \rightarrow E_R} \frac{\mu k_0}{4\pi^2} (E - E_R) T_{ii}(E) = \left| \frac{\mu_j k_{R,i}}{4\pi^2} \langle k_{R,i} | \hat{V} | \phi \rangle^2 \right|. \quad (24)$$

Here, E_R and $k_{R,i}$ denote the energy and momentum of the pole in the i -th channel. In this work, we extract the residue of the T -matrix using the CSM and verify the results using the Complex Scaled Lippmann-Schwinger Equation (CSLSE) [71].

In the CSM framework, while the ratios between par-

tial widths for broad resonances are accurate, the absolute magnitudes may not be precise [72]. Typically, the partial widths (or residues) are determined by combining the total width (from the pole's imaginary part) with the calculated branching ratios. Based on the residue ratios, distinct coupling patterns emerge for the two poles found in the coupled $D^*\bar{D}'_1(^1,^5P_1)$ sector. The first pole couples predominantly to the 1P_1 channel, while the second couples mainly to the 5P_1 channel. We also calculated the wave function probabilities for these poles, obtaining $(88.2 + 6.4i, 11.8 - 6.4i)\%$ for the first pole and $(15.2 - 1.3i, 84.8 + 1.3i)\%$ for the second. These component probabilities are consistent with the residue analysis.

The pole positions and behaviors in the $D^*\bar{D}_1$ sector are largely similar to those in the $D^*\bar{D}'_1$ sector. In the

System	Threshold	$\left[E, \frac{\mu k_{R,i}}{4\pi^2} ResT \right]_{Inst}$	$\left[E, \frac{\mu k_{R,i}}{4\pi^2} ResT \right]_{SL}$	$\left[E, \frac{\mu k_{R,i}}{4\pi^2} ResT \right]_{SE}$
$\{D\bar{D}_0^*\}(^1P_1)$	4210.3	$[-25.9 - 31.7i, (20.4)]$	$[-21.6 - 26.1i, (19.1)]$	$[8.7 - 184.2i, (45.7)]$
$\{D\bar{D}_1'\}(^3P_1)$	4279.3	$[-21.7 - 33.5i, (22.4)]$	$[-21.6 - 26.3i, (17.3)]$	$[3.4 - 131.0i, (34.3)]$
$\{D\bar{D}_1\}(^3P_1)$	4289.4	$[-23.1 - 32.4i, (21.8)]$	$[-20.6 - 27.8i, (17.7)]$	$[-15.0 - 42.4i, (16.3)]$
$[D\bar{D}_2^*](^5P_1)$	4328.4	$[-24.0 - 32.8i, (23.0)]$	$[-23.8 - 30.8i, (21.1)]$	$[-9.8 - 78.0i, (25.6)]$
$[D^*\bar{D}_0^*](^3P_1)$	4351.6	$[-20.4 - 32.6i, (21.9)]$	$[-18.5 - 31.5i, (21.4)]$	$[17.6 - 195.1i, (51.3)]$
$[D^*\bar{D}_1'](^1P_1, ^5P_1)$	4420.6	$\left\{ \begin{array}{l} [-16.5 - 29.6i, (17.3, 3.3)] \\ [-51.0 - 31.6i, (3.4, 25.3)] \end{array} \right.$	$\left[\begin{array}{l} [-11.8 - 21.2i, (12.4, 7.8)] \\ [-34.1 - 20.8i, (5.7, 18.7)] \end{array} \right]$	$\left[\begin{array}{l} [13.7 - 128.9i, (30.4, 17.1)] \\ [-19.7 - 126.0i, (11.2, 32.9)] \end{array} \right]$
$\{D^*\bar{D}_1\}(^3P_1)$	4420.6	$[-22.3 - 33.6i, (21.7)]$	$[-23.1 - 34.2i, (21.7)]$	$[3.0 - 141.6i, (36.4)]$
$[D^*\bar{D}_1(^1P_1, ^5P_1)]$	4430.7	$\left\{ \begin{array}{l} [-25.5 - 32.4i, (18.3, 5.1)] \\ [-15.1 - 22.9i, (4.2, 14.4)] \end{array} \right.$	$\left[\begin{array}{l} [-25.1 - 30.7i, (18.0, 4.3)] \\ [-14.7 - 23.1i, (4.1, 15.3)] \end{array} \right]$	$\left[\begin{array}{l} [-20.2 - 45.0i, (27.5, 3.9)] \\ [-9.4 - 37.9i, (3.9, 16.1)] \end{array} \right]$
$\{D^*\bar{D}_1\}(^3P_1)$	4430.7	$[-28.6 - 36.3i, (25.5)]$	$[-27.6 - 34.0i, (23.9)]$	$[-22.5 - 48.4i, (22.2)]$
$D^*\bar{D}_2^*(^3P_1, ^5P_1)$	4469.7	$\left\{ \begin{array}{l} [-24.8 - 37.1i, (17.8, 19.0)] \\ [-23.4 - 28.5i, (15.5, 15.9)] \end{array} \right.$	$\left[\begin{array}{l} [-21.6 - 29.7i, (21.2, 1.5)] \\ [-30.8 - 35.3i, (1.5, 21.5)] \end{array} \right]$	$\left[\begin{array}{l} [-8.1 - 76.1i, (26.5, 2.0)] \\ [-18.7 - 81.2i, (1.6, 22.6)] \end{array} \right]$

TABLE VI. The extracted poles of the P -wave systems with $I^G(J^{PC}) = 1^+(1^{+-})$ using a cutoff $\Lambda = 0.6$ GeV. The values $\left[E, \frac{\mu k_{R,i}}{4\pi^2} |ResT| \right]$ represent the pole energy E and the residue of the T -matrix, respectively. The data (in units of MeV) in the column “Inst” are obtained under the instantaneous approximation ($q_0 = 0$). The column “SL” refers to the static limit using the q_0 values from Table IV. The column “SE” further includes the self-energy contributions based on the static limit settings.

$D^*\bar{D}_2^*$ sector, two poles also emerge; however, they are closer in energy, and the residue ratios between their respective coupled channels are approximately 1:1, indicating strong mixing.

B. The static limit and self-energy diagram correction

We now proceed to incorporate three-body effects by considering the cross-diagrams in the OPE potential and the self-energy contributions of the constituent mesons.

The results calculated under the static limit approximation are presented in the fourth column of Table VI. Compared to the instantaneous approximation scheme, both the eigenenergies and residues show observable shifts. To isolate the impact of the OPE-induced three-body effect, we use the $\{D\bar{D}_1'\}(^3P_1)$, $\{D\bar{D}_1\}(^3P_1)$, and $[D^*\bar{D}_0^*](^3P_1)$ diagonal potentials as baselines; these channels lack OPE contributions and thus are free from OPE-mediated three-body decay. In contrast, the $\{D\bar{D}_0^*\}(^1P_1)$ and $[D\bar{D}_2^*](^5P_1)$ channels contain OPE terms with significant energy transfer. However, the variations in their pole positions and residues are comparable to those in the non-OPE channels. This suggests that while the static limit correction (manifested as non-zero q_0) does influence the pole behavior, the specific contribution from the OPE-induced three-body decay is relatively minor.

We further examine the influence of the static limit approximation on sectors with spin-mixing. For the $[D^*\bar{D}_1(^1P_1, ^5P_1)]$ system, the pole behavior remains

largely unchanged. In contrast, the $[D^*\bar{D}_1'](^1P_1, ^5P_1)$ system exhibits more noticeable shifts in energy and residue ratios. In the $D^*\bar{D}_2^*(^3P_1, ^5P_1)$ system, while the two poles separate only slightly, their residues exhibit a remarkable change. Combining this with the calculated component probabilities— $(105.5 - 5.2i, -5.5 + 5.2i)\%$ for the first pole and $(-5.5 + 5.3i, 105.5 - 5.3i)\%$ for the second—we conclude that the first (second) pole has effectively decoupled from the 5P_1 (3P_1) channel in the static limit approximation.

Building upon the static limit, we next incorporate the self-energy effects of the unstable mesons D_0^* , D_1' , D_1 , and D_2^* . As indicated in Eq. (8), we explicitly include the imaginary part of the self-energy, treating the real part as a perturbation. The decay width formulas for these charmed mesons are provided in Appendix VID, assuming that the widths are dominated by two-body strong decays involving a pion. The resulting pole parameters are listed in the fifth column (“SE”) of Table VI.

Consider the pole in the $\{D\bar{D}_0^*\}(^1P_1)$ channel. Its energy shifts dramatically compared to the previous two schemes: the real part moves from below to above the threshold, and the imaginary part increases significantly, far exceeding the value without self-energy corrections. Clearly, there is a positive correlation between the large width of the constituent D_0^* (229 MeV) and the final width of the molecular state. A similar pattern is observed in other systems composed of broad mesons like D_1' : the widths are amplified drastically, resulting in broad near-threshold resonances. Given the large exper-

Pole	E (MeV)	Properties (%)	$\frac{\mu k_{R,i}}{4\pi^2} \text{Res}T $ (MeV)
Pole A	$4461.0 - 75.7i$	$\left\{ \begin{array}{l} (0, -0.1 - 0.1i, 0, 0, 0, \\ 0, 0.1i, 0.2 + 0.8i, 0.3, 0.2 - 0.2i, \\ -0.6i, 0.1i, -0.2i, \mathbf{115.2 - 18.8i}, \mathbf{-15.8 + 18.9i}) \end{array} \right.$	$(0.4, 0.2, 0, 4.3, 0.2, \\ 0.7, 0.8, 0.6, 2.6, 1.5, \\ 0.1, 0.2, 0.1, \mathbf{28.4}, \mathbf{5.9})$
$\{D\bar{D}_0^*\}$ Pole	$4211.0 - 177.9i$	$\left\{ \begin{array}{l} (-0.1 - 0.2i, 0.8 + 0.2i, \mathbf{64.6 + 16.7i}, -1.8 - 0.3i, -0.3 - 0.3i, \\ -0.2i, -1.6 + 0.3i, 2.0 + 0.8i, -0.1 + 0.5i, 5.9 + 0.5i, \\ 22.4 - 25.0i, 3.5 + 8.6i, 6.1 - 5.4i, -1.2 + 4.5i, -0.2 - 0.8i) \end{array} \right.$	$(1.7, 2.0, \mathbf{203.0}, 1.1, 1.0, \\ 0.5, 0.1, 0.7, 0.1, 1.2, \\ 7.9, 1.5, 3.3, 2.0, 0.8)$

TABLE VII. The eigenenergies, component probabilities (Properties), and T -matrix residues of the representative candidate poles calculated in the full 15 coupled-channel space. “Pole A” corresponds to the $Z_c(4430)$ candidate identified in the $D^*\bar{D}_2^*$ sector (see the bolded entry in Table VI), while “ $\{D\bar{D}_0^*\}$ Pole” corresponds to the $Z_c(4200)$ candidate in the $\{D\bar{D}_0^*\}$ sector (see the first row of Table VI). The dominant components are highlighted in bold.

imental uncertainties of the $Z_c(4200)$, the broad resonances in both the $\{D\bar{D}_0^*\}(^1P_1)$ and $\{D\bar{D}'_1\}(^3P_1)$ sectors fall within a reasonable range to be considered as candidates.

For systems containing the relatively narrower D_1 and D_2^* , the real parts of the poles move closer to the threshold but remain below it, while the imaginary parts increase correspondingly with the widths of these constituents. Notably, the $D^*\bar{D}_2^*(^3P_1, ^5P_1)$ and $D^*\bar{D}_1(^{1,3,5}P_1)$ sectors host multiple broad poles with masses and widths comparable to the $Z_c(4430)$, making them all viable molecular candidates. Given the coexistence of these overlapping resonances, in experimental observations of final states such as $\psi(2S)\pi$ or $D^*\bar{D}\pi$, significant interference effects—either constructive or destructive—are expected. However, since the relative phases and production strengths of these poles cannot be determined within the current framework, we do not perform a quantitative analysis of the total line shape that includes interference effects. Instead, to illustrate the line shape features and open-charm decay ratios characteristic of such broad molecular candidates, we select the first pole in the $D^*\bar{D}_2^*(^3P_1, ^5P_1)$ system ($E = -8.1 - 76.1i$ MeV) as a representative case. We denote this pole as **Pole A** and will discuss its decay process and line shape in the next subsection.

Finally, to validate our single-channel analysis, we performed a full coupled-channel calculation involving all 15 channels (see Table II) for the representative candidate poles identified above. The resulting energies, component probabilities, and T -matrix residues are listed in Table VII. Comparing these results with the single-sector calculations, the pole positions show minimal deviation. For Pole A (the $Z_c(4430)$ candidate), the properties and T -matrix residues are dominated by the $D^*\bar{D}_2^*(^3P_1, ^5P_1)$ channels. Similarly, for the $\{D\bar{D}_0^*\}$ pole (the $Z_c(4200)$ candidate), the dynamics are dominated by the $\{D\bar{D}_0^*\}(^1P_1)$ channel. In conclusion, our analysis justifies the use of the single-sector approximation—specifically $D^*\bar{D}_2^*(^3P_1, ^5P_1)$ and $\{D\bar{D}_0^*\}(^1P_1)$ —for studying these potential exotic states, as the influence of other coupled channels is negligible.

C. Line shape of the $Z_c(4430)$ Candidate

To further investigate the properties of the $Z_c(4430)$ under the molecular hypothesis, we proceed to analyze the decay processes and spectral line shape, assuming it corresponds to the $D^*\bar{D}_2^*$ resonance (Pole A). We construct the effective Lagrangian describing the coupling between the resonance (Z) and the $D^*\bar{D}_2^*/\bar{D}^*D_2^*$ channels:

$$\mathcal{L}_Z = g_{Z_1} \varepsilon^{\alpha\beta\mu\nu} Z_{\mu\nu}^i \tau_{ab}^i \partial_\beta \tilde{D}_b^{*\gamma\dagger} \tilde{D}_{2a\alpha\gamma}^{*\dagger} + g_{Z_2} \varepsilon^{\alpha\beta\mu\nu} Z_{\mu\nu}^i \tau_{ab}^i \partial^\gamma \tilde{D}_{b\beta}^{*\dagger} \tilde{D}_{2a\alpha\gamma}^{*\dagger} + h.c., \quad (25)$$

where the field strength tensor is defined as $\mathcal{Z}_{\mu\nu} = \partial_\mu Z_\nu - \partial_\nu Z_\mu$, and Z_μ represents the field corresponding to the $D^*\bar{D}_2^*$ molecular state.

Derived from this effective Lagrangian, the energy-dependent partial decay width for the process $Z_c \rightarrow D^*\bar{D}_2^*$ is expressed as:

$$\Gamma_{D^*\bar{D}_2^*}(E) = \frac{20}{9\pi} m_Z m_{D^*} m_{D_2^*} \left[|g_{Z_1}|^2 + |g_{Z_2}|^2 \frac{m_Z^2}{m_{D_2^*}^2} - \text{Re}(g_{Z_1}^* g_{Z_2}) \frac{m_Z}{m_{D_2^*}} \right] p^3 \left(\frac{\Lambda^2}{\Lambda^2 + p^2} \right)^2 \quad (26)$$

where p denotes the magnitude of the relative momentum in the center-of-mass frame. To account for the finite size of the hadrons and regularize contributions from the high-momentum region, a monopole form factor $\mathcal{F}(p^2) = \frac{\Lambda^2}{\Lambda^2 + p^2}$ is introduced at the interaction vertex.

We adopt the parameters of Pole A listed in Table VI. The transition amplitude $\langle k_{R,i} | \hat{V} | \phi \rangle$ is extracted via the CSM. By utilizing the ratio of the transition amplitudes into the $(^3P_1)$ and $(^5P_1)$ channels, we determine the coupling ratio $g_{Z_2}/g_{Z_1} = 0.130 - 0.035i$.

Since the traditional Breit-Wigner distribution is often inadequate for such a broad, near-threshold system, we characterize the resonance line shape using a Flatté-like parameterization. This approach incorporates an energy-dependent self-energy function $\Sigma(E)$ in the denominator to preserve analyticity. In terms of the bare mass m_0 and

the coupling constant g_{Z_1} , the differential cross-section takes the form:

$$\frac{d\sigma}{dE} = C \left| \frac{m_0 \sqrt{\Gamma_{in} \Gamma_f(E)}}{E^2 - m_0^2 - m_0 \Sigma(E) + i m_0 \Gamma_{D_2^*}(E)} \right|^2, \quad (27)$$

where $\Gamma_f(E)$ is the energy-dependent partial width for a specific final state, and C is a normalization constant. Γ_{in} represents the partial width into the incoming channel; since the production mechanism is not specified, we treat it as an effective constant near the $D^* \bar{D}_2^*$ threshold. $\Gamma_{D_2^*}(E)$ represents the energy-dependent width of the unstable constituent D_2^* , as given in Eqs. (87)-(88). Including this term accounts for the additional width contribution inherited from the instability of the D_2^* constituent.

The imaginary part of the self-energy is determined by the optical theorem:

$$\text{Im}\Sigma(E) = -\Gamma_{D^* \bar{D}_2^*}(E). \quad (28)$$

The real part, $\text{Re}\Sigma(E)$, is then derived from the imaginary part via the unsubtracted dispersion relation:

$$\text{Re}\Sigma(E) = \frac{1}{\pi} \mathcal{P} \int_{E_{th}}^{\infty} \frac{\text{Im}\Sigma(E')}{E' - E} dE', \quad (29)$$

where $E_{th} = m_{D^*} + m_{D_2^*}$ is the threshold of the open-charm channel. It is worth noting that the form factor introduced in Eq. (27) (implicitly in the width) ensures the convergence of the integral at the high-energy limit. This dispersive approach guarantees that the real and imaginary parts of the self-energy satisfy the Kramers-Kronig relations, thereby preserving the analyticity of the scattering amplitude.

We determine the parameters of the Flatté-like distribution by aligning the complex pole position with the theoretical energy E_R of Pole A, while simultaneously fitting the peak of the line shape to the experimental central value of the $Z_c(4430)$ [63]. This matching procedure leads to the selection of the cutoff parameter $\Lambda = 0.35$ GeV and determines the remaining parameters as: $m_0 = 4526.9$ MeV, $g_{Z_1} = 0.417$ GeV $^{-5/2}$, and $g_{Z_2} = 0.054 - 0.015$ GeV $^{-5/2}$.

Considering the positively charged state Z_c^+ , the two-body modes are $D^{*+} \bar{D}_2^{*0}$ and $D_2^{*+} \bar{D}^{*0}$. The relevant three-body modes include $D^{*+} \bar{D}^- \pi^+$, $D^0 \bar{D}^{*0} \pi^+$, $D^{*+} \bar{D}^0 \pi^0$, $D^+ \bar{D}^{*0} \pi^0$, $D^{*+} \bar{D}^{*-} \pi^+$, $D^{*0} \bar{D}^{*0} \pi^+$, and $D^{*+} \bar{D}^{*0} \pi^0$. Based on isospin symmetry and the decay branching fractions of the excited mesons, we derive the following relations:

$$\begin{aligned} \Gamma(A \rightarrow D^{*+} \bar{D}_2^{*0}) &= \Gamma(A \rightarrow D_2^{*+} \bar{D}^{*0}), \\ \Gamma(A \rightarrow D^{*+} D^- \pi^+) &= \Gamma(A \rightarrow D^0 \bar{D}^{*0} \pi^+), \\ &= 2\Gamma(A \rightarrow D^{*+} \bar{D}^0 \pi^0) = 2\Gamma(A \rightarrow D^+ \bar{D}^{*0} \pi^0), \\ \Gamma(A \rightarrow D^{*+} D^{*-} \pi^+) &= \Gamma(A \rightarrow D^{*0} \bar{D}^{*0} \pi^+). \end{aligned} \quad (30)$$

The $D^{*+} \bar{D}^{*0} \pi^0$ channel involves quantum interference between two sequential decay diagrams:

$$i\mathcal{M} = i\mathcal{M}(A \rightarrow D^{*+} \bar{D}_2^{*0} \rightarrow D^{*+} \bar{D}^{*0} \pi^0)$$

$$+ i\mathcal{M}(A \rightarrow D_2^{*+} \bar{D}^{*0} \rightarrow D^{*+} \bar{D}^{*0} \pi^0). \quad (31)$$

In Fig. 4, we plot the energy-dependent differential cross-sections, $\frac{1}{C} \frac{d\sigma}{dE}$, for both the two-body and three-body open-charm final states. The incoming width parameter is fixed to the total width of Pole A, i.e., $\Gamma_{in} = 152$ MeV. For comparison, we also include the hidden-charm decay mode $A \rightarrow \psi(2S) \pi^+$, assuming an S-wave effective width $\Gamma_{\psi'}(E) = g_{\psi'} |\vec{p}_\pi|$. This channel is of particular interest as it corresponds to the discovery mode of the $Z_c(4430)$ and is theoretically expected to be favored due to the substantial spatial overlap between the extended P -wave molecular state and the radially excited $\psi(2S)$ [45]. Since the effective coupling $g_{\psi'}$ cannot be rigorously determined within the current framework, we calibrate its value by normalizing the peak of the $\psi(2S) \pi^+$ line shape to match the maximum height of the dominant $D^{*+} \bar{D}_2^{*0}$ mode. This approach facilitates a direct comparison of their spectral structures—specifically the width and threshold behaviors—without implying a quantitative prediction of their relative branching fractions. The figure also displays the line shapes for the representative three-body modes $D^{*+} D^- \pi^+$, $D^{*+} D^{*-} \pi^+$, and $D^{*+} \bar{D}^{*0} \pi^0$. The distributions for other final states can be inferred from the isospin relations in Eq. (30).

The line shapes exhibit distinct features governed by their respective kinematic regimes. For the hidden-charm channel $\psi(2S) \pi^+$, which lies far above its threshold, the phase space factor varies slowly. Consequently, the distribution is dominated by the modulus squared of the resonance propagator. Interestingly, the apparent width of this peak is approximately 80 MeV, which is noticeably narrower than the intrinsic pole width ($\Gamma \approx 152$ MeV). This narrowing arises from the energy-dependent self-energy $\Sigma(E)$ in the denominator, which is significantly suppressed by the form factor with the soft cutoff ($\Lambda = 0.35$ GeV) in the high-energy region.

Similarly, the open-charm line shapes are governed by the interplay between threshold kinematics and the hadronic form factor. The low-energy behavior is suppressed by the P -wave phase space ($\propto p^3$), leading to a delayed rise in the cross-section. Meanwhile, the high-energy tail is directly damped by the vertex form factor. This combined effect results in an asymmetric open-charm peak with an apparent width that is comparable to the hidden-charm mode but topologically distinct. It is crucial to emphasize that while the apparent spectral widths in both channels are narrowed by the regularization scheme, the extracted pole width (~ 150 MeV) remains in good agreement with the experimental value (~ 180 MeV).

Finally, the differential cross-sections for the three-body final states (e.g., $D^{*+} \bar{D}^{*0} \pi^0$) shown in Fig. 4(b) exhibit similar asymmetric structures to the two-body open-charm mode. These distributions arise from the subsequent decay of the unstable D_2^* component and confirm that the broad resonant signature of the $Z_c(4430)$ candidate is preserved in the experimentally observable multi-body final states.

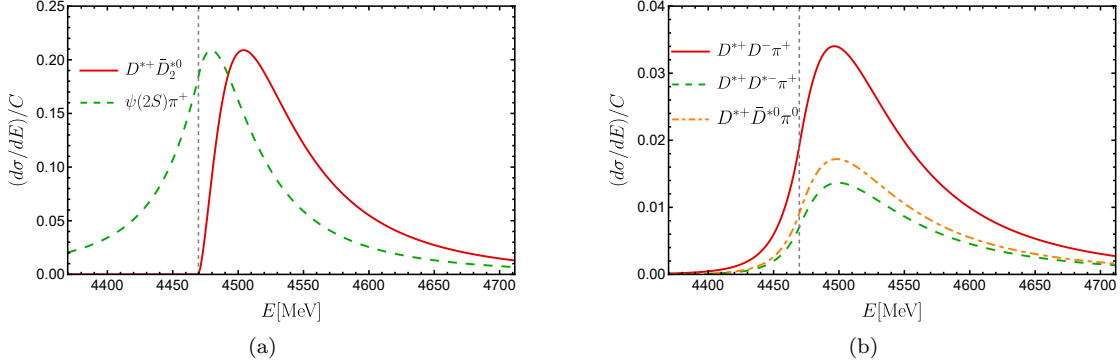


FIG. 4. Production line shapes of resonance A (corresponding to the $Z_c(4430)$ candidate) decaying into (a) two-body final states $D^{*+}\bar{D}_2^{*0}$ and $\psi(2S)\pi^+$, and (b) three-body final states $D^{*+}D^-\pi^+$, $D^{*+}D^-\pi^+$, and $D^{*+}\bar{D}^{*0}\pi^0$. The coupling constant $g_{\psi'}$ is determined by scaling the $\psi(2S)\pi^+$ distribution to share the same peak height as the $D^{*+}\bar{D}_2^{*0}$ mode, serving solely for shape comparison.

V. SUMMARY

In this study, we employ the OBE potential to investigate the hidden-charm tetraquark states with $I^G(J^{PC}) = 1^+(1^{+-})$ within the molecular picture. The constituents include the S -wave (D, D^*) doublet and the P -wave (D_0^*, D_1') and (D_1, D_2^*) doublets. In total, 10 sectors are examined, comprising 7 single-channel systems: $\{D\bar{D}^*\}(^3S_1)$, $D^*\bar{D}^*(^3S_1)$, $\{D\bar{D}_0^*\}(^1P_1)$, $\{D\bar{D}_1'\}(^3P_1)$, $\{D\bar{D}_1\}(^3P_1)$, $[D\bar{D}_2^*](^5P_1)$, and $[D^*\bar{D}_0^*](^3P_1)$; and 3 coupled-channel systems exhibiting spin-mixing: $D^*\bar{D}_1'(^{1,3,5}P_1)$, $D^*\bar{D}_1(^{1,3,5}P_1)$, and $D^*\bar{D}_2^*(^{3,5}P_1)$.

We constructed the effective Lagrangians based on Heavy Quark Symmetry and chiral symmetry. By matching the invariant amplitudes from the quark model with those at the hadronic level, we determined the necessary coupling constants, which show excellent agreement with experimental data. In the study of molecular systems with Z_c -like quantum numbers, we observed that the potentials from ρ and ω exchanges largely cancel each other, leaving the medium- and long-range interactions dominated by π and σ exchanges.

We solved the Schrödinger equation in momentum space using the CSM and verified the results via the CSLSE. Consequently, we treated the (D, D^*) mesons as stable particles, focusing on the P -wave molecular states formed by their combinations with the unstable (D_0^*, D_1') and (D_1, D_2^*) mesons. Initially, using $g_\sigma = 2.73$, we re-evaluated the S -wave molecular candidates corresponding to T_{cc} , $X(3872)$, $G(3900)$, and $Z_c(3900)$ from our previous work [61], confirming that the qualitative conclusions remain unchanged. Subsequently, under the instantaneous approximation ($q_0 = 0$), we found that a sub-threshold resonance emerges in every P -wave system, while systems with spin-mixing exhibit two sub-threshold resonances. These results are consistent with expectations from heavy quark spin symmetry. Upon in-

corporating the static limit correction (finite q_0), the pole positions shifted, with changes in the imaginary parts on the order of a few MeV.

Finally, the inclusion of the self-energy contributions led to drastic changes in the pole parameters; specifically, the increase in the imaginary parts is positively correlated with the widths of the constituent P -wave charmed hadrons. Notably, the broad resonances identified in the $D^*\bar{D}_1$, $D^*\bar{D}_2^*$, $\{D\bar{D}_0^*\}$, and $\{D\bar{D}_1'\}$ sectors exhibit masses and widths comparable to the exotic states $Z_c(4430)$ and $Z_c(4200)$, suggesting multiple possible molecular assignments. Taking the $D^*\bar{D}_2^*(^{3,5}P_1)$ and $\{D\bar{D}_0^*\}(^1P_1)$ sectors as prime examples, we demonstrated that the three-body effects significantly amplify their widths, bringing the calculated parameters into excellent agreement with experimental values.

In Subsection IV C, we analyzed the line shape of the $Z_c(4430)$ candidate (assuming the $D^*\bar{D}_2^*$ assignment) using a Flatté-like parameterization that incorporates self-energy corrections derived from CSM amplitudes. We compared the line shapes for the open-charm ($D^*\bar{D}_2^*$ and three-body) and hidden-charm ($\psi(2S)\pi$) channels. Our results show that the open-charm structures are located above the $D^*\bar{D}_2^*$ threshold and exhibit distinct asymmetric line shapes governed by the P -wave phase space and the form factor. Crucially, although the apparent spectral widths in both channels are compressed by the regularization scheme, the extracted pole width is consistent with the experimental observation.

In summary, we have applied the OBE model to investigate P -wave molecules composed of a negative-parity meson ($D^{(*)}$) and a positive-parity meson (D_0^*, D_1', D_1, D_2^*). We conclude that these systems universally support broad, near-threshold resonances, and that three-body decay effects play a critical role in determining their widths and pole positions. The theoretical framework and results presented here, particularly the relations for open-charm decay channels, serve as a valuable guide for future experimental searches for hidden-charm

tetraquarks in three-body final states such as $D^* \bar{D}^* \pi$ and $D^* \bar{D} \pi$.

ACKNOWLEDGMENTS

This work was supported in part by the National Natural Science Foundation of China under Grants No. 12405160, No. 12547101, No. 11975033, No. 12147168, No. 12070131001, No. 12105072, No. 12475137, and No. 12405088. J. B. Cheng is also supported by the Fundamental Research Funds for the Central Universities (Grant No. 23CX06061A), the Shandong Provincial Natural Science Foundation, China (Grant No. ZR2024QA041). J. Z. Wang is also supported by the Start-up Funds of Chongqing University.

VI. APPENDIX

A. Appendix A: Expanded Interaction Lagrangians

After expanding the Lagrangian in Eq. (13), we obtain the effective Lagrangians describing the interactions of heavy flavor mesons with light mesons. The effective Lagrangian for pseudoscalar meson (π, η) exchanges is given by:

$$\begin{aligned}
\mathcal{L}_{P^*P\mathcal{M}} &= -\frac{2g}{f_\pi}(P_b P_{a\mu}^{*\dagger} + P_{b\mu}^* P_a^\dagger) \partial^\mu \mathcal{M}_{ba}, \\
\mathcal{L}_{P^*P^*\mathcal{M}} &= i\frac{2g}{f_\pi} \varepsilon_{\alpha\mu\nu\lambda} v^\alpha P_b^{*\mu} P_a^{*\nu\dagger} \partial^\lambda \mathcal{M}_{ba}, \\
\mathcal{L}_{P'_1P_0^*\mathcal{M}} &= -\frac{2g'}{f_\pi}(P_{1b}^\mu P_{0a}^{*\dagger} + P_{0b}^* P_{1a}^{\mu\dagger}) \partial_\mu \mathcal{M}_{ba}, \\
\mathcal{L}_{P'_1P'_1\mathcal{M}} &= \frac{2ig'}{f_\pi} \varepsilon_{\alpha\mu\nu\lambda} v^\alpha P_{1b}^{\mu\dagger} P_{1a}^{\nu\dagger} \partial^\lambda \mathcal{M}_{ba}, \\
\mathcal{L}_{P_1P_1\mathcal{M}} &= -\frac{5ig''}{3f_\pi} \varepsilon_{\alpha\mu\nu\lambda} v^\alpha P_{1b}^\mu P_{1a}^{\nu\dagger} \partial^\lambda \mathcal{M}_{ba}, \\
\mathcal{L}_{P_1P_2^*\mathcal{M}} &= -\sqrt{\frac{2}{3}} \frac{g''}{f_\pi} (P_{2b}^{*\mu\nu} P_{1a\mu}^\dagger + P_{1b}^\mu P_{2a\mu}^{*\nu\dagger}) \partial_\nu \mathcal{M}_{ba}, \\
\mathcal{L}_{P_2^*P_2^*\mathcal{M}} &= \frac{2ig''}{f_\pi} \varepsilon_{\alpha\mu\nu\lambda} v^\alpha P_{2b}^{*\beta\mu} P_{2a\beta}^{*\nu\dagger} \partial^\lambda \mathcal{M}_{ba}, \\
\mathcal{L}_{PP_0^*\mathcal{M}} &= \frac{2f''}{f_\pi} (P_{0b}^* P_a^\dagger + P_b P_{0a}^{*\dagger}) v_\alpha \partial^\alpha \mathcal{M}_{ba}, \\
\mathcal{L}_{P^*P'_1\mathcal{M}} &= -\frac{2f''}{f_\pi} (P_{1b}^{\mu\dagger} P_{a\mu}^{*\dagger} + P_{b\mu}^* P_{1a}^{\mu\dagger}) v_\alpha \partial^\alpha \mathcal{M}_{ba}, \\
\mathcal{L}_{PP_2^*\mathcal{M}} &= -\frac{2i(h_1 + h_2)}{\Lambda_\chi f_\pi} (P_{2b}^{*\mu\nu} P_a^\dagger - P_b P_{2a}^{*\mu\nu\dagger}) \partial_\mu \partial_\nu \mathcal{M}_{ba}, \\
\mathcal{L}_{P^*P_1\mathcal{M}} &= -\sqrt{\frac{2}{3}} \frac{i(h_1 + h_2)}{\Lambda_\chi f_\pi} [3g_{\mu\nu} g_{\alpha\beta} + g_{\nu\beta}(-g_{\mu\alpha} + v_\mu v_\alpha)] \\
&\quad \times (P_{1b}^\nu P_a^{*\beta\dagger} - P_b^{*\beta} P_{1a}^{\nu\dagger}) \partial^\mu \partial^\alpha \mathcal{M}_{ba}, \\
\mathcal{L}_{P^*P_2^*\mathcal{M}} &= \frac{2(h_1 + h_2)}{\Lambda_\chi f_\pi} \varepsilon_{\rho\nu\alpha\beta} v^\rho \partial_\mu \partial^\alpha \mathcal{M}_{ba} (P_{2b}^{*\mu\nu} P_a^{*\beta\dagger} + P_b^{*\beta} P_{2a}^{*\mu\nu\dagger}),
\end{aligned}$$

$$\begin{aligned}
\mathcal{L}_{P_0^*P_1\mathcal{M}} &= -\sqrt{\frac{2}{3}} \frac{2f'}{f_\pi} (P_{1b}^\mu P_{0a}^{*\dagger} + P_{0b}^* P_{1a}^{\mu\dagger}) \partial_\mu \mathcal{M}_{ba}, \\
\mathcal{L}_{P'_1P_1\mathcal{M}} &= -\sqrt{\frac{2}{3}} \frac{if'}{f_\pi} \varepsilon_{\alpha\mu\nu\lambda} v^\alpha (P_{1b}^\mu P_{1a}^{\nu\dagger} + P_{1b}^{\nu\dagger} P_{1a}^\mu) \partial^\lambda \mathcal{M}_{ba}, \\
\mathcal{L}_{P'_1P_2\mathcal{M}} &= \frac{2f'}{f_\pi} (P_{2b}^{*\mu\nu} P_{1a\nu}^{*\dagger} + P_{1b}^{\nu\dagger} P_{2a\nu}^{*\mu\dagger}) \partial_\mu \mathcal{M}_{ba}. \quad (32)
\end{aligned}$$

The effective Lagrangian for scalar meson (σ) exchanges is given by:

$$\begin{aligned}
\mathcal{L}_{PP\sigma} &= -2g_\sigma P_a^\dagger P_a \sigma, \\
\mathcal{L}_{P^*P^*\sigma} &= 2g_\sigma P_{a\mu}^{*\dagger} P_a^{*\mu} \sigma, \\
\mathcal{L}_{P_0^*P_0^*\sigma} &= 2g'_\sigma P_{0a}^{*\dagger} P_{0a}^* \sigma, \\
\mathcal{L}_{P'_1P'_1\sigma} &= -2g'_\sigma P_{1a\mu}^\dagger P_{1a}^{\mu\dagger} \sigma, \\
\mathcal{L}_{P_1P_1\sigma} &= -2g''_\sigma P_{1a\mu}^\dagger P_{1a}^\mu \sigma, \\
\mathcal{L}_{P_2^*P_2^*\sigma} &= 2g''_\sigma P_{2a\mu\nu}^{*\dagger} P_{2a}^{*\mu\nu} \sigma, \\
\mathcal{L}_{PP'_1\sigma} &= -\frac{2ih_\sigma}{f_\pi} (P_a^\dagger P_{1a}^{\mu\dagger} - P_{1a}^{\mu\dagger} P_a) \partial_\mu \sigma, \\
\mathcal{L}_{P^*P_0^*\sigma} &= -\frac{i2h_\sigma}{f_\pi} (P_a^{*\mu\dagger} P_{0a}^* - P_{0a}^{*\dagger} P_a^*) \partial_\mu \sigma, \\
\mathcal{L}_{P^*P'_1\sigma} &= \frac{2h_\sigma}{f_\pi} \varepsilon_{\lambda\mu\nu\alpha} v^\lambda (P_a^{*\mu\dagger} P_{1a}^\nu - P_{1a}^{\mu\dagger} P_a^{*\nu}) \partial^\alpha \sigma, \\
\mathcal{L}_{PP_1\sigma} &= -2\sqrt{\frac{2}{3}} \frac{ih'_\sigma}{f_\pi} (P_a^\dagger P_{1a}^{\mu\dagger} - P_{1a}^{\mu\dagger} P_a) \partial_\mu \sigma, \\
\mathcal{L}_{P^*P_1\sigma} &= -\sqrt{\frac{2}{3}} \frac{h'_\sigma}{f_\pi} \varepsilon_{\lambda\mu\nu\alpha} v^\lambda (P_a^{*\mu\dagger} P_{1a}^\nu - P_{1a}^{\mu\dagger} P_a^{*\nu}) \partial^\alpha \sigma, \\
\mathcal{L}_{P^*P_2^*\sigma} &= \frac{2ih'_\sigma}{f_\pi} (P_{a\mu}^{*\dagger} P_{2a}^{*\mu\nu} - P_{2a}^{*\mu\nu\dagger} P_{a\mu}^*) \partial_\nu \sigma. \quad (33)
\end{aligned}$$

The effective Lagrangian for vector meson (ρ, ω) exchanges describing intra-multiplet interactions is:

$$\begin{aligned}
\mathcal{L}_{PPV} &= -\sqrt{2} \beta g_V P_b P_a^\dagger v \cdot \hat{\rho}_{ba}, \\
\mathcal{L}_{PP^*V} &= -2\sqrt{2} \lambda g_V \varepsilon_{\lambda\alpha\mu\nu} v^\lambda (P_b P_a^{*\alpha\dagger} + P_b^{*\alpha} P_a^\dagger) \partial^\mu \hat{\rho}_{ba}^\nu, \\
\mathcal{L}_{P^*P^*V} &= \sqrt{2} \beta g_V P_b^{*\mu} P_{a\mu}^{*\dagger} v \cdot \hat{\rho}_{ba} \\
&\quad - 2\sqrt{2} i \lambda g_V P_b^{*\mu} P_a^{*\nu\dagger} (\partial_\mu \hat{\rho}_\nu - \partial_\nu \hat{\rho}_\mu)_{ba}, \\
\mathcal{L}_{P_0^*P_0^*\mathcal{V}} &= \sqrt{2} \beta_1 g_V P_{0b}^* P_{0a}^{*\dagger} v \cdot \hat{\rho}_{ba}, \\
\mathcal{L}_{P_0^*P'_1\mathcal{V}} &= 2\sqrt{2} \lambda_1 g_V \varepsilon_{\lambda\alpha\mu\nu} v^\lambda (P_{0b}^* P_{1a}^{\alpha\dagger} + P_{1b}^{\alpha\dagger} P_{0a}^*) \partial^\mu \hat{\rho}_{ba}^\nu, \\
\mathcal{L}_{P'_1P'_1\mathcal{V}} &= -\sqrt{2} \beta_1 g_V P_{1b}^{\mu\dagger} P_{1a\mu}^\dagger v \cdot \hat{\rho}_{ba} \\
&\quad + 2\sqrt{2} i \lambda_1 g_V P_{1b}^{\mu\dagger} P_{1a}^{\nu\dagger} (\partial_\mu \hat{\rho}_\nu - \partial_\nu \hat{\rho}_\mu)_{ba}, \\
\mathcal{L}_{P_1P_1\mathcal{V}} &= -\sqrt{2} \beta_2 g_V P_{1b}^\mu P_{1a\mu}^\dagger (v \cdot \hat{\rho})_{ba} \\
&\quad + i \frac{5}{3} \sqrt{2} \lambda_2 g_V P_{1b}^\mu P_{1a}^{\nu\dagger} (\partial_\mu \hat{\rho}_\nu - \partial_\nu \hat{\rho}_\mu)_{ba}, \\
\mathcal{L}_{P_1P_2^*\mathcal{V}} &= -\frac{2}{\sqrt{3}} \lambda_2 g_V \varepsilon_{\lambda\alpha\mu\nu} v^\lambda \\
&\quad \times \left[(P_{2b}^{*\sigma\alpha} P_{1a\sigma}^\dagger + P_{1b\sigma} P_{2a}^{*\sigma\alpha\dagger}) (\partial^\mu \hat{\rho}^\nu)_{ba} \right. \\
&\quad \left. - (P_{2b}^{*\sigma\mu} P_{1a}^{\nu\dagger} + P_{1b}^\nu P_{2a}^{*\sigma\mu\dagger}) (\partial_\sigma \hat{\rho}^\alpha)_{ba} \right],
\end{aligned}$$

$$\begin{aligned} \mathcal{L}_{P_2^* P_2^* \mathcal{V}} &= \sqrt{2} \beta_2 g_V P_{2b}^{*\mu\nu} P_{2a\mu\nu}^{*\dagger} (v \cdot \hat{\rho})_{ba} \\ &\quad - 2\sqrt{2} i \lambda_2 g_V P_{2b}^{*\sigma\mu} P_{2a\sigma}^{*\nu\dagger} (\partial_\mu \hat{\rho}_\nu - \partial_\nu \hat{\rho}_\mu)_{ba}. \end{aligned} \quad (34)$$

The mixing terms between the ground-state doublets and the P -wave excited doublets are:

$$\begin{aligned} \mathcal{L}_{PP_1' \mathcal{V}} &= -\sqrt{2} \zeta g_V (P_b P_{1a}^{\prime\mu\dagger} + P_{1b}^{\prime\mu} P_a^\dagger) (\hat{\rho}_\mu)_{ba} \\ &\quad - 2\sqrt{2} i \mu g_V v^\mu (P_b P_{1a}^{\prime\nu\dagger} - P_{1b}^{\prime\nu} P_a^\dagger) \\ &\quad \times (\partial_\mu \hat{\rho}_\nu - \partial_\nu \hat{\rho}_\mu)_{ba}, \\ \mathcal{L}_{P^* P_0^* \mathcal{V}} &= -\sqrt{2} \zeta g_V (P_b^{*\mu} P_{0a}^{*\dagger} + P_{0b}^* P_a^{*\mu\dagger}) (\hat{\rho}_\mu)_{ba} \\ &\quad - 2\sqrt{2} i \mu g_V v^\mu (P_b^{*\nu} P_{0a}^{*\dagger} - P_{0b}^* P_a^{*\nu\dagger}) \\ &\quad \times (\partial_\mu \hat{\rho}_\nu - \partial_\nu \hat{\rho}_\mu)_{ba}, \\ \mathcal{L}_{P^* P_1' \mathcal{V}} &= \sqrt{2} \zeta g_V i \varepsilon_{\lambda\mu\nu\alpha} v^\lambda (P_b^{*\mu} P_{1a}^{\prime\nu\dagger} + P_{1b}^{\prime\mu} P_a^{*\nu\dagger}) (\hat{\rho}^\alpha)_{ba} \\ &\quad - \sqrt{2} \mu g_V \varepsilon_{\alpha\beta\mu\nu} (P_b^{*\alpha} P_{1a}^{\prime\beta\dagger} - P_{1b}^{\prime\alpha} P_a^{*\beta\dagger}) \\ &\quad \times (\partial^\mu \hat{\rho}^\nu - \partial^\nu \hat{\rho}^\mu)_{ba}, \\ \mathcal{L}_{PP_1 \mathcal{V}} &= -\frac{2}{\sqrt{3}} \zeta_1 g_V (P_{1b}^\mu P_a^\dagger + P_b P_{1a}^{\mu\dagger}) (\hat{\rho}_\mu)_{ba} \\ &\quad - i \frac{2}{\sqrt{3}} \mu_1 g_V v^\mu (P_{1b}^\nu P_a^\dagger - P_b P_{1a}^{\nu\dagger}) \\ &\quad \times (\partial_\mu \hat{\rho}_\nu - \partial_\nu \hat{\rho}_\mu)_{ba}, \\ \mathcal{L}_{P^* P_1 \mathcal{V}} &= -\frac{1}{\sqrt{3}} \zeta_1 g_V i \varepsilon_{\lambda\mu\nu\alpha} v^\lambda (P_{1b}^\mu P_a^{\nu\dagger} + P_b^* P_{1a}^{\mu\nu\dagger}) (\hat{\rho}^\alpha)_{ba} \\ &\quad + \frac{1}{\sqrt{3}} \mu_1 g_V v_\mu v^\sigma \varepsilon_{\sigma\nu\alpha\beta} (P_{1b}^\alpha P_a^{\nu\beta\dagger} - P_b^* P_{1a}^{\alpha\nu\dagger}) \\ &\quad \times (\partial^\mu \hat{\rho}^\nu - \partial^\nu \hat{\rho}^\mu)_{ba}, \\ \mathcal{L}_{P^* P_2^* \mathcal{V}} &= \sqrt{2} \zeta_1 g_V (P_{2b}^{*\mu\nu} P_{a\nu}^{*\dagger} + P_{b\nu}^* P_{2a}^{*\mu\nu\dagger}) (\hat{\rho}_\mu)_{ba} \\ &\quad - i \sqrt{2} \mu_1 g_V v^\mu (P_{2b}^{*\nu\alpha} P_{a\alpha}^{*\dagger} - P_{b\alpha}^* P_{2a}^{*\nu\alpha\dagger}) \\ &\quad \times (\partial_\mu \hat{\rho}_\nu - \partial_\nu \hat{\rho}_\mu)_{ba}. \end{aligned} \quad (35)$$

Finally, the mixing terms between different P -wave multiplets are:

$$\begin{aligned} \mathcal{L}_{P_0^* P_1 \mathcal{V}} &= \frac{2}{\sqrt{3}} \mu_2 g_V \varepsilon_{\alpha\beta\mu\nu} v^\alpha (P_{1b}^\beta P_{0a}^{*\dagger} + P_{0b}^* P_{1a}^{\beta\dagger}) \partial^\mu \hat{\rho}^\nu, \\ \mathcal{L}_{P_1' P_1 \mathcal{V}} &= -i \frac{1}{\sqrt{3}} \mu_2 g_V (P_{1b}^\mu P_{1a}^{\nu\dagger} + P_{1b}^{\prime\mu} P_{1a}^{\nu\dagger}) \\ &\quad \times (\partial_\mu \hat{\rho}_\nu - \partial_\nu \hat{\rho}_\mu)_{ba}, \\ \mathcal{L}_{P_1' P_2^* \mathcal{V}} &= -\sqrt{2} \mu_2 g_V \varepsilon_{\sigma\nu\alpha\beta} v^\sigma (P_{2b\mu}^{*\alpha} P_{1a}^{\prime\beta\dagger} + P_{1b}^{\prime\beta} P_{2a\mu}^{\alpha\dagger}) \\ &\quad \times (\partial^\mu \hat{\rho}^\nu - \partial^\nu \hat{\rho}^\mu)_{ba}. \end{aligned} \quad (36)$$

The interaction terms not explicitly listed are zero.

The Lagrangians for the anti-charmed hadrons can be derived from those of the charmed sector via the charge conjugation (C) transformation. The transformation properties for the heavy meson fields are given by:

$$\begin{aligned} P_a &\xrightarrow{C} \tilde{P}_a, & P_a^* &\xrightarrow{C} -\tilde{P}_a^*, \\ P_{0a}^* &\xrightarrow{C} \tilde{P}_{0a}^*, & P_{1a}^{\prime\mu} &\xrightarrow{C} \tilde{P}_{1a}^{\prime\mu}, \\ P_{1a} &\xrightarrow{C} \tilde{P}_{1a}, & P_{2a}^* &\xrightarrow{C} -\tilde{P}_{2a}^*. \end{aligned} \quad (37)$$

For the light mesons, the fields transform as follows:

$$\mathcal{M} \xrightarrow{C} \mathcal{M}^T, \quad \hat{\rho} \xrightarrow{C} -\hat{\rho}^T, \quad \sigma \xrightarrow{C} \sigma. \quad (38)$$

B. Appendix B: coupling constants

In this appendix, we detail the determination of the coupling constants associated with the $(0^-, 1^-)$, $(0^+, 1^+)$, and $(1^+, 2^+)$ heavy meson doublets. We employ the quark model combined with experimental data to systematically estimate these parameters.

The effective Lagrangian describing the interactions of the light constituent quarks (u, d) is given by

$$\begin{aligned} \mathcal{L}_q &= -\frac{g_A}{\sqrt{2} f_\pi} \bar{\psi} \gamma^\mu \gamma_5 \partial_\mu (\pi^i \tau^i) \psi - g_\sigma^q \bar{\psi} \sigma \psi \\ &\quad - g_\rho^q \bar{\psi} \gamma^\mu (\rho_\mu^i \tau^i + \omega_\mu) \psi - f_\rho^q \bar{\psi} \sigma^{\mu\nu} \partial_\mu (\rho_\nu^i \tau^i + \omega_\nu) \psi \end{aligned} \quad (39)$$

Under the assumption that the heavy quark acts as a spectator and does not participate in the coupling with light mesons, we can derive the relations between the coupling constants at the hadronic and quark levels by matching the transition matrix elements calculated in both frameworks. Taking the classic process $D^* \rightarrow D\pi$ as an example, the invariant amplitude at the hadronic level is

$$\begin{aligned} i\mathcal{M}_H[D^{*0}(m_J = 0) \rightarrow D^+(m_J' = 0)\pi^-] \\ = \frac{g}{f_\pi} \epsilon_\mu(m_J = 0) q^\mu = -\frac{g}{f_\pi} q^3, \end{aligned} \quad (40)$$

where m_J (m_J') denotes the third component of the total angular momentum of the initial (final) heavy meson, and \vec{q} represents the pion momentum. On the other hand, the invariant amplitude at the quark level is expressed as

$$\begin{aligned} i\mathcal{M}_Q(\bar{u} \rightarrow \bar{d}\pi^-) &= \frac{g_A}{f_\pi} \left[\chi_{\bar{u}}^\dagger (\vec{\sigma} \cdot \vec{q}) \chi_{\bar{d}} \right] \\ &\quad - \frac{g_A}{f_\pi} q^0 \left[\chi_{\bar{u}}^\dagger \vec{\sigma} \cdot \left(\frac{\vec{p}'}{2m_d} + \frac{\vec{p}}{2m_u} \right) \chi_{\bar{d}} \right], \end{aligned} \quad (41)$$

where $\chi_{\bar{u}}$ ($\chi_{\bar{d}}$) is the Pauli spinor of the \bar{u} (\bar{d}) antiquark, and m_u (m_d) and \vec{p} (\vec{p}') are the mass and momentum of the \bar{u} (\bar{d}) antiquark in the heavy quark rest frame, satisfying $\vec{q} = \vec{p} - \vec{p}'$. Since $|q^0| \ll m_u \approx 400$ MeV for the $D^* \rightarrow D\pi$ process, the first term dominates the amplitude in Eq. (41). Consequently, the corresponding amplitude at the quark level becomes

$$\begin{aligned} i\mathcal{M}_Q[D^{*0}(m_J = 0) \rightarrow D^+(m_J' = 0)\pi^-] \\ = \langle \Psi_{m_J' = 0}(D^+) | \frac{g_A}{f_\pi} (\vec{\sigma} \cdot \vec{q}) | \Psi_{m_J = 0}(D^{*0}) \rangle, \end{aligned} \quad (42)$$

where the wave function of the D^* meson is decomposed as $|\Psi_{m_J}(D^{*0})\rangle = \sum_{lm\lambda} |\psi_{lm}(D^{*0})\rangle |\chi_\lambda(D^{*0})\rangle$. Specifically, the spatial part is $|\psi_{lm}(D^{*0})\rangle = |\psi_{00}(D^{*0})\rangle$, and the spin part is $|\chi_\lambda(D^{*0})\rangle = |\chi_0(D^{*0})\rangle = \frac{1}{\sqrt{2}} (\uparrow\downarrow + \downarrow\uparrow)$

$\otimes c\bar{u}$. The operator $\vec{\sigma} \cdot \vec{q}$ acts only on the spin wave function, leading to

$$\begin{aligned} \langle \vec{\sigma} \cdot \vec{q} \rangle &= \sum_{lm\lambda; l'm'\lambda'} \langle \psi_{l'm'}(D^+) | \psi_{lm}(D^{*0}) \rangle \\ &\quad \langle \chi_{\lambda'}(D^+) | \vec{\sigma} \cdot \vec{q} | \chi_{\lambda}(D^{*0}) \rangle \\ &= \int \frac{d^3 p}{(2\pi)^3} \psi_{00}^*(\vec{p}', D^+) \psi_{00}(\vec{p}, D^{*0})(q^3). \end{aligned} \quad (43)$$

Considering the limited phase space of the $D^* \rightarrow D\pi$ process, we have $|\vec{q}| \ll |\vec{p}|, |\vec{p}'|$, where $|\vec{p}| \approx 400$ MeV in the heavy quark effective theory [73]. This implies $\vec{p}' \approx \vec{p}$ and $\psi_{00}^*(\vec{p}', D^+) \approx \psi_{00}^*(\vec{p}, D^+)$. In the heavy quark limit, we assume identical spatial wave functions for the D and D^* mesons, yielding the overlap integral $\int \frac{d^3 p}{(2\pi)^3} \psi_{00}^*(\vec{p}, D^+) \psi_{00}(\vec{p}, D^{*0}) = 1$. By matching the hadronic level amplitude in Eq. (40) with the quark level result derived from Eqs. (42) and (43), we obtain

$$g = -g_A, \quad (44)$$

where $g_A = 0.75$ is taken from the chiral quark model [74].

We proceed to determine the remaining coupling constants in the OPE interaction. For transitions between two heavy mesons with the same parity, the second term in Eq. (41) is proportional to $\frac{q^0}{2m_u} \langle \vec{\sigma} \cdot \vec{q} \rangle$, which is suppressed relative to the first term $\langle \vec{\sigma} \cdot \vec{q} \rangle$ due to the factor $q^0/2m_u$. Consequently, we can estimate the coupling constants g' , g'' , and f' using a similar approach. We again approximate $\vec{p}' \approx \vec{p}$ in the final state spatial wave function $\psi_{l'm'}^*(\vec{p}')$ to simplify the integral. In Ref. [75], the authors employed a modified Godfrey-Isgur (GI) model where charmed mesons are described by single spherical harmonic oscillator functions $\Psi_{nlm}^{SHO}(\vec{p})$. The quantum numbers $n^{2S+1}L_J$ for the (D, D^*) , (D_0^*, D_1') , and (D_1, D_2^*) doublets are assigned as $(1^1S_0, 1^3S_1)$, $(1^3P_0, 1^3P_1)$, and $(1^1P_1, 1^3P_2)$, respectively. Neglecting the mass differences (or scale parameter variations [75]) within the doublets, the wave functions of heavy mesons with the same parity satisfy the orthonormality condition:

$$\langle \psi_{l'm'}(H'_f) | \psi_{lm}(H_i) \rangle \approx \delta_{l',l} \delta_{m',m}. \quad (45)$$

Based on this, we derive the following relations:

$$g' = g_A/3, \quad g'' = g_A, \quad f' = -\frac{2}{\sqrt{3}}g_A. \quad (46)$$

For transitions involving heavy mesons with different parity, the first term $\langle \vec{\sigma} \cdot \vec{q} \rangle$ in Eq. (41) vanishes due to the orthogonality of the spherical harmonic functions, provided $|\vec{q}| \ll |\vec{p}|, |\vec{p}'|$. However, this condition is not strictly satisfied here. For instance, in the $D_0^* \rightarrow D\pi$ decay, $|\vec{q}| \approx 400$ MeV, which is comparable to the estimated internal momentum $|\vec{p}|$. Thus, this term could yield a non-negligible contribution. Nevertheless, for the

purpose of a rapid estimation in this work, we retain the approximation $\vec{p}' \approx \vec{p}$. Under this assumption, the amplitude in Eq. (41) is dominated by the \vec{p} -dependent term:

$$i\mathcal{M}_Q(\bar{u} \rightarrow \bar{d}\pi^-) = -\frac{g_A}{f_\pi} \frac{q^0}{m_u} \left[\chi_{\bar{u}}^\dagger(\vec{\sigma} \cdot \vec{p}) \chi_{\bar{d}} \right]. \quad (47)$$

To simplify the subsequent expressions for coupling constants, we define a general overlap integral $\mathcal{I}(H_a, H_b)$ as:

$$\mathcal{I}(H_a, H_b) = \frac{1}{(2\pi)^3} \int_0^\infty dp p^3 \phi_{L_a}(p, H_a) \phi_{L_b}^*(p, H_b), \quad (48)$$

where $\phi_L(p, H)$ denotes the radial wave function of hadron H in momentum space. By calculating the spin operator matrix element of $\langle \vec{\sigma} \rangle$ and performing the solid angle integration over \vec{p} , we obtain:

$$\begin{aligned} f'' &= \frac{1}{3} \frac{g_A}{m_u} \mathcal{I}(D_0^*, D), \\ \frac{h_1 + h_2}{\Lambda_\chi} &= \frac{1}{4\sqrt{3}} \frac{g_A}{m_u^2} \mathcal{I}(D_2^*, D). \end{aligned} \quad (49)$$

Using the constituent quark mass $m_q = 340$ MeV and the model parameters corresponding to $\mu = 0.03$ from Table II of Ref. [75], we calculate:

$$f'' = 1.00g_A, \quad (h_1 + h_2)/\Lambda_\chi = 0.89g_A \text{ GeV}^{-1}. \quad (50)$$

Alternatively, f'' and $(h_1 + h_2)/\Lambda_\chi$ can be extracted from the experimental widths of D_0^* and D_1 . Assuming the open-charm channels dominate their widths, i.e., $\Gamma_{D_0^*} = \frac{3}{2}\Gamma(D_0^* \rightarrow D\pi^+)$ and $\Gamma_{D_1} = \frac{3}{2}\Gamma(D_1 \rightarrow D^*\pi^+)$, and using the average masses from Table I, we obtain $|f''| = 0.53$ and $|(h_1 + h_2)/\Lambda_\chi| = 1.22 \text{ GeV}^{-1}$. Additionally, averaging the values extracted from D_1 and D_2^* yields $|(h_1 + h_2)/\Lambda_\chi| = 1.03 \text{ GeV}^{-1}$. Evidently, these phenomenological values are consistent with the quark model predictions.

The final coupling constants for pion exchange are determined by combining the magnitude from experimental data with the sign predicted by the quark model. Consequently, the adopted values are $g = -0.59$ (magnitude from [76]), $g' = 0.25$, $g'' = 0.75$, $f' = -0.87$, $f'' = 0.53$, and $(h_1 + h_2)/\Lambda_\chi = 1.03 \text{ GeV}^{-1}$.

For vector meson interactions, the couplings are derived similarly using the definition in Eq. (48):

$$\begin{aligned} \lambda_{GV} &= -f_\rho^q, \quad \lambda_1 g_{GV} = -f_\rho^q/3, \quad \lambda_2 g_{GV} = f_\rho^q, \\ \beta g_{GV} &= -2g_\rho^q, \quad \beta_1 g_{GV} = 2g_\rho^q, \quad \beta_2 g_{GV} = 2g_\rho^q, \\ \zeta g_{GV} &= -\frac{2}{3} \frac{g_\rho^q}{m_u} \mathcal{I}(D_1', D), \quad \mu g_{GV} = \frac{2}{3} \frac{f_\rho^q}{m_u} \mathcal{I}(D_1', D), \\ \zeta_1 g_{GV} &= -\frac{2}{\sqrt{3}} \frac{g_\rho^q}{m_u} \mathcal{I}(D_1, D), \quad \mu_1 g_{GV} = \frac{2}{\sqrt{3}} \frac{f_\rho^q}{m_u} \mathcal{I}(D_1, D), \\ \mu_2 g_{GV} &= 4f_\rho^q/\sqrt{3}. \end{aligned} \quad (51)$$

We take $g_V = 5.8$, $\beta = 0.9$, and $\lambda = 0.56 \text{ GeV}^{-1}$ [77, 78] as inputs to determine the other vector coupling constants: $\lambda_1 = 0.19 \text{ GeV}^{-1}$, $\lambda_2 = -0.56 \text{ GeV}^{-1}$,

$\beta_1 = -0.90$, $\beta_2 = -0.90$, $\mu = -1.00 \text{ GeV}^{-1}$, $\mu_1 = -1.74 \text{ GeV}^{-1}$, $\mu_2 = -1.29 \text{ GeV}^{-1}$, $\zeta = 0.81$ and $\zeta_1 = 1.40$.

For scalar meson interactions, we obtain:

$$\begin{aligned} g_\sigma &= g_\sigma^q, \quad g'_\sigma = -g_\sigma^q, \quad g''_\sigma = -g_\sigma^q, \\ h_\sigma &= \frac{1}{6} \frac{f_\pi g_\sigma^q}{m_u^2} \mathcal{I}(D'_1, D), \quad h'_\sigma = -\frac{1}{4\sqrt{3}} \frac{f_\pi g_\sigma^q}{m_u^2} \mathcal{I}(D_1, D). \end{aligned} \quad (52)$$

Adopting the chiral quark model [74] and the Goldberger-Treiman relation [79], we set $g_\sigma^q = g_{\pi qq} \approx m_q g_A/f_\pi = 2.73$. The corresponding coupling constants are $g_\sigma = 2.73$, $g'_\sigma = -2.73$, $g''_\sigma = -2.73$, $h_\sigma = 0.48$, and $h'_\sigma = -0.48$.

C. Appendix C: potential

For simplicity, we first derive the OBE potential for a system of two charmed mesons (e.g., DD^*) prior to partial wave decomposition. Subsequently, we apply the G-parity transformation to both the heavy and light mesons to obtain the complete potential for the hidden-charm sector. Taking the $PP^* \rightarrow PP^*$ process as an illustrative example, the OBE potential is given by:

$$\begin{aligned} V(DD^* \rightarrow DD^*) &= V_\pi^D + V_\pi^C + V_\eta + V_\eta^D + V_\eta^C + V_\sigma^D \\ &\quad + V_\sigma^C + V_\rho^D + V_\rho^C + V_\omega^D + V_\omega^C, \\ V_\pi^D &= V_\eta^D = V_\sigma^C = 0, \\ V_\pi^C &= \frac{g^2}{2f_\pi^2} \frac{(\vec{q} \cdot \vec{\epsilon}_3^\dagger)(\vec{q} \cdot \vec{\epsilon}_1)}{q^2 - m_\pi^2} \vec{\tau}_1 \cdot \vec{\tau}_2, \end{aligned}$$

$$\begin{aligned} V_\eta^C &= \frac{g^2}{6f_\pi^2} \frac{(\vec{q} \cdot \vec{\epsilon}_3^\dagger)(\vec{q} \cdot \vec{\epsilon}_1)}{q^2 - m_\eta^2}, \quad V_\sigma^D = g_\sigma^2 \frac{\vec{\epsilon}_4^\dagger \cdot \vec{\epsilon}_2}{q^2 - m_\sigma^2}, \\ V_\rho^D &= -\frac{1}{4} \beta^2 g_V^2 \frac{\vec{\epsilon}_4^\dagger \cdot \vec{\epsilon}_2}{q^2 - m_\rho^2} \vec{\tau}_1 \cdot \vec{\tau}_2, \\ V_\rho^C &= \lambda^2 g_V^2 \frac{\vec{q}^2 (\vec{\epsilon}_3^\dagger \cdot \vec{\epsilon}_2) - (\vec{q} \cdot \vec{\epsilon}_3^\dagger)(\vec{q} \cdot \vec{\epsilon}_2)}{q^2 - m_\rho^2} \vec{\tau}_1 \cdot \vec{\tau}_2, \\ V_\omega^D &= -\frac{1}{4} \beta^2 g_V^2 \frac{\vec{\epsilon}_4^\dagger \cdot \vec{\epsilon}_2}{q^2 - m_\omega^2}, \\ V_\omega^C &= \lambda^2 g_V^2 \frac{\vec{q}^2 (\vec{\epsilon}_3^\dagger \cdot \vec{\epsilon}_2) - (\vec{q} \cdot \vec{\epsilon}_3^\dagger)(\vec{q} \cdot \vec{\epsilon}_2)}{q^2 - m_\omega^2}. \end{aligned} \quad (53)$$

where $\vec{\epsilon}$ ($\vec{\epsilon}^\dagger$) denotes the polarization vector of the initial (final) D^* meson. V^D and V^C correspond to the direct diagram ($DD^* \rightarrow DD^*$) and the cross diagram ($DD^* \rightarrow D^*D$), respectively.

We then consider the G-parity transformations: $D \xrightarrow{G} -\bar{D}$, $D^* \xrightarrow{G} \bar{D}^*$, $D_0^* \xrightarrow{G} -\bar{D}_0^*$, $D'_1 \xrightarrow{G} -\bar{D}'_1$, $D_1 \xrightarrow{G} -\bar{D}_1$, $D_2^* \xrightarrow{G} \bar{D}_2^*$, $\pi \xrightarrow{G} -\pi$, $\eta \xrightarrow{G} \eta$, $\sigma \xrightarrow{G} \sigma$, $\rho \xrightarrow{G} \rho$, and $\omega \xrightarrow{G} -\omega$. Taking the first channel $\{D\bar{D}^*\}(^3S_1)$ in Table II as an example, the flavor configuration $\{A\bar{B}\} = (A\bar{B} + B\bar{A})/\sqrt{2}$ or $[A\bar{B}] = (A\bar{B} - B\bar{A})/\sqrt{2}$ introduces a phase factor δ_C in the cross-channel diagrams under G-parity transformation. This factor depends on the symmetry of the final state: $\delta_C = 1$ for $\{A\bar{B}\}$ and $\delta_C = -1$ for $[A\bar{B}]$. For the process $\{D\bar{D}^*\}(^3S_1) \rightarrow \{D\bar{D}^*\}(^3S_1)$, we have $\delta_C = 1$. Consequently, the OBE potential components transform as:

$$\begin{aligned} V(D\bar{D}^* \rightarrow D\bar{D}^*) &= \delta_C \frac{g^2}{2f_\pi^2} (\vec{q} \cdot \vec{\epsilon}_3^\dagger)(\vec{q} \cdot \vec{\epsilon}_2) \left(\frac{\vec{\tau}_1 \cdot \vec{\tau}_2}{q^2 - m_\pi^2} - \frac{1/3}{q^2 - m_\eta^2} \right) + g_\sigma^2 \frac{\vec{\epsilon}_4^\dagger \cdot \vec{\epsilon}_2}{q^2 - m_\sigma^2} \\ &\quad + g_V^2 \left\{ -\frac{1}{4} \beta^2 (\vec{\epsilon}_4^\dagger \cdot \vec{\epsilon}_2) - \delta_C \lambda^2 \left[\vec{q}^2 (\vec{\epsilon}_3^\dagger \cdot \vec{\epsilon}_2) - (\vec{q} \cdot \vec{\epsilon}_3^\dagger)(\vec{q} \cdot \vec{\epsilon}_2) \right] \right\} \left(\frac{\vec{\tau}_1 \cdot \vec{\tau}_2}{q^2 - m_\rho^2} - \frac{1}{q^2 - m_\omega^2} \right), \end{aligned} \quad (54)$$

$$\begin{aligned} V(D^*\bar{D}^* \rightarrow D^*\bar{D}^*) &= -\frac{g^2}{2f_\pi^2} [\vec{q} \cdot (i\vec{\epsilon}_3^\dagger \times \vec{\epsilon}_1)] [\vec{q} \cdot (i\vec{\epsilon}_4^\dagger \times \vec{\epsilon}_2)] \left(\frac{\vec{\tau}_1 \cdot \vec{\tau}_2}{q^2 - m_\pi^2} - \frac{1/3}{q^2 - m_\eta^2} \right) + g_\sigma^2 \frac{(\vec{\epsilon}_3^\dagger \cdot \vec{\epsilon}_1)(\vec{\epsilon}_4^\dagger \cdot \vec{\epsilon}_2)}{q^2 - m_\sigma^2} \\ &\quad + g_V^2 \left\{ -\frac{1}{4} \beta^2 (\vec{\epsilon}_3^\dagger \cdot \vec{\epsilon}_1)(\vec{\epsilon}_4^\dagger \cdot \vec{\epsilon}_2) + \lambda^2 \{ \vec{q}^2 (i\vec{\epsilon}_3^\dagger \times \vec{\epsilon}_1) \cdot (i\vec{\epsilon}_4^\dagger \times \vec{\epsilon}_2) - [\vec{q} \cdot (i\vec{\epsilon}_3^\dagger \times \vec{\epsilon}_1)] [\vec{q} \cdot (i\vec{\epsilon}_4^\dagger \times \vec{\epsilon}_2)] \} \right\} \\ &\quad \times \left(\frac{\vec{\tau}_1 \cdot \vec{\tau}_2}{q^2 - m_\rho^2} - \frac{1}{q^2 - m_\omega^2} \right), \end{aligned} \quad (55)$$

$$V(D\bar{D}_0^* \rightarrow D\bar{D}_0^*) = -\delta_C \frac{f''^2}{2f_\pi^2} q_{0C}^2 \left(\frac{\vec{\tau}_1 \cdot \vec{\tau}_2}{q^2 - m_\pi^2} - \frac{1/3}{q^2 - m_\eta^2} \right) - g_\sigma g'_\sigma \frac{1}{q^2 - m_\sigma^2} + \frac{1}{4} \beta \beta_1 g_V^2 \left(\frac{\vec{\tau}_1 \cdot \vec{\tau}_2}{q^2 - m_\rho^2} - \frac{1}{q^2 - m_\omega^2} \right), \quad (56)$$

$$\begin{aligned} V(D\bar{D}'_1 \rightarrow D\bar{D}'_1) &= -g_\sigma g'_\sigma \frac{\vec{\epsilon}_4^\dagger \cdot \vec{\epsilon}_2}{q^2 - m_\sigma^2} + \delta_C \frac{h_\sigma^2}{f_\pi^2} \frac{(\vec{q} \cdot \vec{\epsilon}_3^\dagger)(\vec{q} \cdot \vec{\epsilon}_2)}{q^2 - m_\sigma^2} + \frac{1}{4} \beta \beta_1 g_V^2 (\vec{\epsilon}_4^\dagger \cdot \vec{\epsilon}_2) \left(\frac{\vec{\tau}_1 \cdot \vec{\tau}_2}{q^2 - m_\rho^2} - \frac{1}{q^2 - m_\omega^2} \right) \\ &\quad + \delta_C g_V^2 \left\{ \frac{1}{4} (\zeta - 2\mu q_{0C})^2 (\vec{\epsilon}_3^\dagger \cdot \vec{\epsilon}_2) - \mu^2 (\vec{q} \cdot \vec{\epsilon}_3^\dagger)(\vec{q} \cdot \vec{\epsilon}_2) \right\} \left(\frac{\vec{\tau}_1 \cdot \vec{\tau}_2}{q^2 - m_\rho^2} - \frac{1}{q^2 - m_\omega^2} \right), \end{aligned} \quad (57)$$

$$\begin{aligned}
V(D\bar{D}_1 \rightarrow D\bar{D}_1) &= -g_\sigma g''_\sigma \frac{\vec{\epsilon}_4^\dagger \cdot \vec{\epsilon}_2}{q^2 - m_\sigma^2} + \delta_C \frac{2}{3} \frac{h_\sigma'^2}{f_\pi^2} \frac{(\vec{q} \cdot \vec{\epsilon}_3^\dagger)(\vec{q} \cdot \vec{\epsilon}_2)}{q^2 - m_\sigma^2} - \frac{1}{4} \beta \beta_2 g_V^2 (\vec{\epsilon}_4^\dagger \cdot \vec{\epsilon}_2) \left(\frac{\vec{\tau}_1 \cdot \vec{\tau}_2}{q^2 - m_\rho^2} - \frac{1}{q^2 - m_\omega^2} \right) \\
&+ \delta_C \frac{g_V^2}{6} \left\{ (\zeta_1 + \mu q_{0C})^2 (\vec{\epsilon}_3^\dagger \cdot \vec{\epsilon}_2) - \mu_1^2 (\vec{q} \cdot \vec{\epsilon}_3^\dagger)(\vec{q} \cdot \vec{\epsilon}_2) \right\} \left(\frac{\vec{\tau}_1 \cdot \vec{\tau}_2}{q^2 - m_\rho^2} - \frac{1}{q^2 - m_\omega^2} \right), \tag{58}
\end{aligned}$$

$$\begin{aligned}
V(D\bar{D}_2^* \rightarrow D\bar{D}_2^*) &= \delta_C \frac{(h_1 + h_2)^2}{2\Lambda_\chi^2 f_\pi^2} (\eta_{3ij}^\dagger q_i q_j) (\eta_{2lm}^\dagger q_l q_m) \left(\frac{\vec{\tau}_1 \cdot \vec{\tau}_2}{q^2 - m_\pi^2} - \frac{1/3}{q^2 - m_\eta^2} \right) - g_\sigma g''_\sigma \frac{\eta_{2ij} \eta_{4ij}^\dagger}{q^2 - m_\sigma^2} \\
&+ \frac{1}{4} \beta \beta_2 g_V^2 (\eta_{2ij} \eta_{4ij}^\dagger) \left(\frac{\vec{\tau}_1 \cdot \vec{\tau}_2}{q^2 - m_\rho^2} - \frac{1}{q^2 - m_\omega^2} \right), \tag{59}
\end{aligned}$$

$$\begin{aligned}
V(D^* \bar{D}_0^* \rightarrow D^* \bar{D}_0^*) &= -g_\sigma g'_\sigma \frac{\vec{\epsilon}_3^\dagger \cdot \vec{\epsilon}_1}{q^2 - m_\sigma^2} - \delta_C \frac{h_\sigma^2}{f_\pi^2} \frac{(\vec{q} \cdot \vec{\epsilon}_4^\dagger)(\vec{q} \cdot \vec{\epsilon}_1)}{q^2 - m_\sigma^2} + \frac{1}{4} \beta \beta_1 g_V^2 (\vec{\epsilon}_3^\dagger \cdot \vec{\epsilon}_1) \left(\frac{\vec{\tau}_1 \cdot \vec{\tau}_2}{q^2 - m_\rho^2} - \frac{1}{q^2 - m_\omega^2} \right) \\
&- \delta_C g_V^2 \left\{ \frac{1}{4} (\zeta - 2\mu q_{0C})^2 (\vec{\epsilon}_4^\dagger \cdot \vec{\epsilon}_1) - \mu^2 (\vec{q} \cdot \vec{\epsilon}_4^\dagger)(\vec{q} \cdot \vec{\epsilon}_1) \right\} \left(\frac{\vec{\tau}_1 \cdot \vec{\tau}_2}{q^2 - m_\rho^2} - \frac{1}{q^2 - m_\omega^2} \right), \tag{60}
\end{aligned}$$

$$\begin{aligned}
V(D^* \bar{D}'_1 \rightarrow D^* \bar{D}'_1) &= -\frac{gg'}{2f_\pi^2} [\vec{q} \cdot (i\vec{\epsilon}_3^\dagger \times \vec{\epsilon}_1)] [\vec{q} \cdot (i\vec{\epsilon}_4^\dagger \times \vec{\epsilon}_2)] \left(\frac{\vec{\tau}_1 \cdot \vec{\tau}_2}{q^2 - m_\pi^2} - \frac{1/3}{q^2 - m_\eta^2} \right) \\
&+ \delta_C \frac{f''^2}{2f_\pi^2} q_{0C}^2 (\vec{\epsilon}_3^\dagger \cdot \vec{\epsilon}_1) (\vec{\epsilon}_4^\dagger \cdot \vec{\epsilon}_2) \left(\frac{\vec{\tau}_1 \cdot \vec{\tau}_2}{q^2 - m_\pi^2} - \frac{1/3}{q^2 - m_\eta^2} \right) - g_\sigma g'_\sigma \frac{(\vec{\epsilon}_3^\dagger \cdot \vec{\epsilon}_1)(\vec{\epsilon}_4^\dagger \cdot \vec{\epsilon}_2)}{q^2 - m_\sigma^2} \\
&- \delta_C \frac{h_\sigma^2}{f_\pi^2} \frac{[\vec{q} \cdot (i\vec{\epsilon}_3^\dagger \times \vec{\epsilon}_1)][\vec{q} \cdot (i\vec{\epsilon}_4^\dagger \times \vec{\epsilon}_2)]}{q^2 - m_\sigma^2} + g_V^2 \left\{ \frac{1}{4} \beta \beta_1 (\vec{\epsilon}_3^\dagger \cdot \vec{\epsilon}_1)(\vec{\epsilon}_4^\dagger \cdot \vec{\epsilon}_2) \right. \\
&\left. - \lambda \lambda_1 \{ \vec{q}^2 (i\vec{\epsilon}_3^\dagger \times \vec{\epsilon}_1) \cdot (i\vec{\epsilon}_4^\dagger \times \vec{\epsilon}_2) - [\vec{q} \cdot (i\vec{\epsilon}_3^\dagger \times \vec{\epsilon}_1)][\vec{q} \cdot (i\vec{\epsilon}_4^\dagger \times \vec{\epsilon}_2)] \} \right\} \left(\frac{\vec{\tau}_1 \cdot \vec{\tau}_2}{q^2 - m_\rho^2} - \frac{1}{q^2 - m_\omega^2} \right) \\
&- \delta_C g_V^2 \left\{ \frac{1}{4} (\zeta - 2\mu q_{0C})^2 [(i\vec{\epsilon}_3^\dagger \times \vec{\epsilon}_1) \cdot (i\vec{\epsilon}_4^\dagger \times \vec{\epsilon}_2)] - \mu^2 [\vec{q} \cdot (i\vec{\epsilon}_3^\dagger \times \vec{\epsilon}_1)][\vec{q} \cdot (i\vec{\epsilon}_4^\dagger \times \vec{\epsilon}_2)] \right\} \\
&\times \left(\frac{\vec{\tau}_1 \cdot \vec{\tau}_2}{q^2 - m_\rho^2} - \frac{1}{q^2 - m_\omega^2} \right), \tag{61}
\end{aligned}$$

$$\begin{aligned}
V(D^* \bar{D}_1 \rightarrow D^* \bar{D}_1) &= \delta_C \frac{3}{2} \frac{(h_1 + h_2)^2}{2\Lambda_\chi^2 f_\pi^2} \left[(\epsilon_{3i}^\dagger \epsilon_{1j} - \frac{1}{3} \delta_{ij} \vec{\epsilon}_3^\dagger \cdot \vec{\epsilon}_1) q_i q_j \right] \left[(\epsilon_{4l}^\dagger \epsilon_{2m} - \frac{1}{3} \delta_{lm} \vec{\epsilon}_4^\dagger \cdot \vec{\epsilon}_2) q_l q_m \right] \left(\frac{\vec{\tau}_1 \cdot \vec{\tau}_2}{q^2 - m_\pi^2} - \frac{1/3}{q^2 - m_\eta^2} \right) \\
&- \frac{5}{6} \frac{gg''}{2f_\pi^2} [\vec{q} \cdot (i\vec{\epsilon}_3^\dagger \times \vec{\epsilon}_1)][\vec{q} \cdot (i\vec{\epsilon}_4^\dagger \times \vec{\epsilon}_2)] \left(\frac{\vec{\tau}_1 \cdot \vec{\tau}_2}{q^2 - m_\pi^2} - \frac{1/3}{q^2 - m_\eta^2} \right) \\
&- g_\sigma g''_\sigma \frac{(\vec{\epsilon}_3^\dagger \cdot \vec{\epsilon}_1)(\vec{\epsilon}_4^\dagger \cdot \vec{\epsilon}_2)}{q^2 - m_\sigma^2} - \delta_C \frac{h_\sigma'^2}{6f_\pi^2} \frac{[\vec{q} \cdot (i\vec{\epsilon}_3^\dagger \times \vec{\epsilon}_1)][\vec{q} \cdot (i\vec{\epsilon}_4^\dagger \times \vec{\epsilon}_2)]}{q^2 - m_\sigma^2} \\
&+ g_V^2 \left\{ \frac{1}{4} \beta \beta_2 (\vec{\epsilon}_3^\dagger \cdot \vec{\epsilon}_1)(\vec{\epsilon}_4^\dagger \cdot \vec{\epsilon}_2) + \frac{1}{2} \lambda \lambda_2 \{ \vec{q}^2 (i\vec{\epsilon}_3^\dagger \times \vec{\epsilon}_1) \cdot (i\vec{\epsilon}_4^\dagger \times \vec{\epsilon}_2) - [\vec{q} \cdot (i\vec{\epsilon}_3^\dagger \times \vec{\epsilon}_1)][\vec{q} \cdot (i\vec{\epsilon}_4^\dagger \times \vec{\epsilon}_2)] \} \right\} \\
&\times \left(\frac{\vec{\tau}_1 \cdot \vec{\tau}_2}{q^2 - m_\rho^2} - \frac{1}{q^2 - m_\omega^2} \right) - \frac{1}{24} \delta_C g_V^2 \left\{ (\zeta_1 + \mu_1 q_{0C})^2 [(i\vec{\epsilon}_3^\dagger \times \vec{\epsilon}_1) \cdot (i\vec{\epsilon}_4^\dagger \times \vec{\epsilon}_2)] \right. \\
&\left. - \mu_1^2 [\vec{q} \cdot (i\vec{\epsilon}_3^\dagger \times \vec{\epsilon}_1)][\vec{q} \cdot (i\vec{\epsilon}_4^\dagger \times \vec{\epsilon}_2)] \right\} \left(\frac{\vec{\tau}_1 \cdot \vec{\tau}_2}{q^2 - m_\rho^2} - \frac{1}{q^2 - m_\omega^2} \right), \tag{62}
\end{aligned}$$

$$\begin{aligned}
V(D^* \bar{D}_2^* \rightarrow D^* \bar{D}_2^*) &= \frac{gg''}{2f_\pi^2} \left\{ [\vec{q} \cdot (i\vec{\epsilon}_3^\dagger \times \vec{\epsilon}_1)] (i \varepsilon_{ijk} \eta_{4li}^\dagger \eta_{2lj} q_k) \right\} \left(\frac{\vec{\tau}_1 \cdot \vec{\tau}_2}{q^2 - m_\pi^2} - \frac{1/3}{q^2 - m_\eta^2} \right) - g_\sigma g''_\sigma \frac{(\vec{\epsilon}_3^\dagger \cdot \vec{\epsilon}_1)(\eta_{4ij}^\dagger \eta_{2ij})}{q^2 - m_\sigma^2} \\
&+ \delta_C \frac{(h_1 + h_2)^2}{2\Lambda_\chi^2 f_\pi^2} (i \varepsilon_{ijk} \epsilon_{1k} \eta_{3in}^\dagger q_j q_n) (i \varepsilon_{i'j'k'} \epsilon_{4k'}^\dagger \eta_{2in'} q_{j'} q_{n'}) \left(\frac{\vec{\tau}_1 \cdot \vec{\tau}_2}{q^2 - m_\pi^2} - \frac{1/3}{q^2 - m_\eta^2} \right)
\end{aligned}$$

$$\begin{aligned}
& + \delta_C \frac{h_\sigma'^2}{f_\pi^2} \frac{(q_i \eta_{3ij}^\dagger \epsilon_{1j})(q_l \eta_{2lm} \epsilon_{4m}^\dagger)}{q^2 - m_\sigma^2} + g_V^2 \left\{ \frac{1}{4} \beta \beta_2 (\vec{\epsilon}_3^\dagger \cdot \vec{\epsilon}_1) (\eta_{4ij}^\dagger \eta_{2ij}) \right. \\
& + \lambda \lambda_2 [\vec{q} \times (\vec{\epsilon}_3^\dagger \times \vec{\epsilon}_1)]_k (\eta_{4ik}^\dagger \eta_{2ij} - \eta_{4ij}^\dagger \eta_{2ik}) q_j \left. \right\} \left(\frac{\vec{\tau}_1 \cdot \vec{\tau}_2}{q^2 - m_\rho^2} - \frac{1}{q^2 - m_\omega^2} \right) \\
& + \delta_C \frac{g_V^2}{4} \left\{ (\zeta_1 - \mu_1 q_{0C})^2 (\eta_{3ik}^\dagger \epsilon_{1i})(\eta_{2jk} \epsilon_{4j}^\dagger) - \mu_1^2 (q_i \eta_{3ij}^\dagger \epsilon_{1j})(q_l \eta_{2lm} \epsilon_{4m}^\dagger) \right\} \\
& \times \left(\frac{\vec{\tau}_1 \cdot \vec{\tau}_2}{q^2 - m_\rho^2} - \frac{1}{q^2 - m_\omega^2} \right). \tag{63}
\end{aligned}$$

In our formalism, $\boldsymbol{\tau}$ denotes the isospin operator represented by the Pauli matrices. We adopt the phase convention where the isospin doublets correspond to the quark pair (u, d) and the antiquark pair $(\bar{d}, -\bar{u})$. Accordingly, the ground state charmed and anti-charmed meson doublets are defined as $(D^{(*)+}, -D^{(*)0})^T$ and $(\bar{D}^{(*)0}, D^{(*)-})^T$, respectively. This convention is consistently applied to the excited P -wave doublets. Under this definition, the isospin factor is given by $\langle \boldsymbol{\tau}_1 \cdot \boldsymbol{\tau}_2 \rangle = 2I(I+1) - 3$. For the isovector Z_c states ($I = 1$) investigated in this work, this yields $\langle \boldsymbol{\tau}_1 \cdot \boldsymbol{\tau}_2 \rangle = 1$.

Here, ϵ^μ represents the polarization vector for D^* , D'_1 , and D_1 mesons, defined as:

$$\epsilon^\mu(\pm 1) = \mp \frac{1}{\sqrt{2}} (0, 1, \pm i, 0)^\mu, \quad \epsilon^\mu(0) = (0, 0, 0, 1)^\mu.$$

The polarization tensor $\eta^{\mu\nu}$ for the D_2^* meson is given by:

$$\begin{aligned}
\eta^{\mu\nu}(\lambda = \pm 2) &= \frac{1}{2} \begin{pmatrix} 0 & 0 & 0 & 0 \\ 0 & 1 & \pm i & 0 \\ 0 & \pm i & -1 & 0 \\ 0 & 0 & 0 & 0 \end{pmatrix}^{\mu\nu}, \\
\eta^{\mu\nu}(\lambda = \pm 1) &= \mp \frac{1}{2} \begin{pmatrix} 0 & 0 & 0 & 0 \\ 0 & 0 & 0 & 1 \\ 0 & 0 & 0 & \pm i \\ 0 & 1 & \pm i & 0 \end{pmatrix}^{\mu\nu}, \\
\eta^{\mu\nu}(\lambda = 0) &= \frac{1}{\sqrt{6}} \begin{pmatrix} 0 & 0 & 0 & 0 \\ 0 & -1 & 0 & 0 \\ 0 & 0 & -1 & 0 \\ 0 & 0 & 0 & 2 \end{pmatrix}^{\mu\nu}. \tag{64}
\end{aligned}$$

The diagonal potentials for channels 1 to 8 after partial wave decomposition are:

$$\begin{aligned}
V_{11}(p', p) &= 2\pi \int_{-1}^1 dt \left\{ \frac{g^2}{2f_\pi^2} \frac{1}{3} (p'^2 + p^2 - 2p'pt) G(\pi, \eta, q_{0C}, p', p, t) + g_\sigma^2 G(m_\sigma, q_{0D}, p', p, t) \right. \\
& \left. - \frac{1}{4} g_V^2 \beta^2 G(\rho, \omega, q_{0D}, p', p, t) - g_V^2 \lambda^2 \frac{2}{3} (p'^2 + p^2 - 2p'pt) G(\rho, \omega, q_{0C}, p', p, t) \right\}, \tag{65}
\end{aligned}$$

$$\begin{aligned}
V_{22}(p', p) &= 2\pi \int_{-1}^1 dt \left\{ \frac{g^2}{2f_\pi^2} \frac{1}{3} (p'^2 + p^2 - 2p'pt) G(\pi, \eta, q_{0C}, p', p, t) + g_\sigma^2 G(m_\sigma, q_{0D}, p', p, t) \right. \\
& \left. - \frac{1}{4} g_V^2 \beta^2 G(\rho, \omega, q_{0D}, p', p, t) - g_V^2 \lambda^2 \frac{2}{3} (p'^2 + p^2 - 2p'pt) G(\rho, \omega, q_{0C}, p', p, t) \right\}, \tag{66}
\end{aligned}$$

$$V_{33}(p', p) = 2\pi \int_{-1}^1 t dt \left\{ - \frac{f''^2}{2f_\pi^2} q_{0C}^2 G(\pi, \eta, q_{0C}, p', p, t) - g_\sigma g'_\sigma G(m_\sigma, q_{0D}, p', p, t) + \frac{1}{4} g_V^2 \beta \beta_1 G(\rho, \omega, q_{0D}, p', p, t) \right\}, \tag{67}$$

$$\begin{aligned}
V_{44}(p', p) &= 2\pi \int_{-1}^1 dt \left\{ - g_\sigma g'_\sigma t G(m_\sigma, q_{0D}, p', p, t) + \frac{h_\sigma^2}{f_\pi^2} \frac{1}{2} p' p (1 - t^2) G(m_\sigma, q_{0C}, p', p, t) \right. \\
& \left. + \frac{1}{4} g_V^2 \beta \beta_1 t G(\rho, \omega, q_{0D}, p', p, t) + g_V^2 \left[\frac{1}{4} (\zeta - 2\mu q_{0C})^2 t - \mu^2 \frac{1}{2} p' p (1 - t^2) \right] G(\rho, \omega, q_{0C}, p', p, t) \right\}, \tag{68}
\end{aligned}$$

$$V_{55}(p', p) = 2\pi \int_{-1}^1 dt \left\{ -g_\sigma g_\sigma'' t G(m_\sigma, q_{0D}, p', p, t) + \frac{2}{3} \frac{h_\sigma'^2}{f_\pi^2} \frac{1}{2} p' p (1-t^2) G(m_\sigma, q_{0C}, p', p, t) \right. \\ \left. - \frac{1}{4} g_V^2 \beta \beta_2 t G(\rho, \omega, q_{0D}, p', p, t) + \frac{g_V^2}{6} \left[(\zeta_1 + \mu q_{0C})^2 t - \mu_1^2 \frac{1}{2} p' p (1-t^2) \right] G(\rho, \omega, q_{0C}, p', p, t) \right\}, \quad (69)$$

$$V_{66}(p', p) = 2\pi \int_{-1}^1 dt \left\{ -\frac{(h_1 + h_2)^2}{2\Lambda_\chi^2 f_\pi^2} \frac{1}{15} \left[4(p'^4 + p^4) t + 2p'^2 p^2 t (7 + 5t^2) - (p'^3 p + p' p^3) (3 + 13t^2) \right] \right. \\ \left. \times G(\pi, \eta, q_{0C}, p', p, t) - g_\sigma g_\sigma'' t G(m_\sigma, q_{0D}, p', p, t) + \frac{1}{4} \beta \beta_2 g_V^2 t G(\rho, \omega, q_{0D}, p', p, t) \right\}, \quad (70)$$

$$V_{77}(p', p) = 2\pi \int_{-1}^1 dt \left\{ -g_\sigma g_\sigma' t G(m_\sigma, q_{0D}, p', p, t) + \frac{h_\sigma^2}{f_\pi^2} \frac{1}{2} p' p (1-t^2) G(m_\sigma, q_{0C}, p', p, t) \right. \\ \left. + \frac{1}{4} \beta \beta_1 g_V^2 t G(\rho, \omega, q_{0D}, p', p, t) + g_V^2 \left[\frac{1}{4} (\zeta - 2\mu q_{0C})^2 t - \mu^2 \frac{1}{2} p' p (1-t^2) \right] G(\rho, \omega, q_{0C}, p', p, t) \right\}, \quad (71)$$

The propagator functions are defined as:

$$G(m, q_0, p', p, t) = \frac{-1}{p'^2 + p^2 - 2p'pt + m^2 - q_0^2}, \\ G(\pi, \eta, q_0, p', p, t) = G(m_\pi, q_0, p', p, t) - \frac{1}{3} G(m_\eta, q_0, p', p, t), \\ G(\rho, \omega, q_0, p', p, t) = G(m_\rho, q_0, p', p, t) - G(m_\omega, q_0, p', p, t). \quad (72)$$

The partial wave projected potentials for $D^* \bar{D}'_1 \rightarrow D^* \bar{D}'_1$ (channels 8–10) are:

$$V_{88}(p', p) = 2\pi \int_{-1}^1 t dt \left\{ -\frac{gg'}{2f_\pi^2} \frac{-2}{3} (p'^2 + p^2 - 2p'pt) G(\pi, \eta, q_{0D}, p', p, t) - \frac{f''^2}{2f_\pi^2} q_{0C}^2 G(\pi, \eta, q_{0C}, p', p, t) \right. \\ \left. - g_\sigma g_\sigma' G(m_\sigma, q_{0D}, p', p, t) + \frac{h_\sigma^2}{f_\pi^2} \frac{-2}{3} (p'^2 + p^2 - 2p'pt) G(m_\sigma, q_{0C}, p', p, t) \right. \\ \left. + g_V^2 \left[\frac{1}{4} \beta \beta_1 + \lambda \lambda_1 \frac{4}{3} (p'^2 + p^2 - 2p'pt) \right] G(\rho, \omega, q_{0D}, p', p, t) \right. \\ \left. + g_V^2 \left[-\frac{1}{2} (\zeta - 2\mu q_{0C})^2 + \mu^2 \frac{2}{3} (p'^2 + p^2 - 2p'pt) \right] G(\rho, \omega, q_{0C}, p', p, t) \right\}, \quad (73)$$

$$V_{99}(p', p) = 2\pi \int_{-1}^1 dt \left\{ \frac{gg'}{2f_\pi^2} \frac{1}{2} (1-t^2) G(\pi, \eta, q_{0D}, p', p, t) + \frac{f''^2}{2f_\pi^2} q_{0C}^2 t G(\pi, \eta, q_{0C}, p', p, t) \right. \\ \left. - g_\sigma g_\sigma' t G(m_\sigma, q_{0D}, p', p, t) + \frac{h_\sigma^2}{f_\pi^2} \frac{1}{2} (1-t^2) G(m_\sigma, q_{0C}, p', p, t) \right. \\ \left. + g_V^2 \left[\frac{1}{4} \beta \beta_1 t - \lambda \lambda_1 \left(-(p'^2 + p^2)t + p' p \frac{1}{2} (1+3t^2) \right) \right] G(\rho, \omega, q_{0D}, p', p, t) \right. \\ \left. - g_V^2 \left[-\frac{1}{4} (\zeta - 2\mu q_{0C})^2 t + \mu^2 \frac{1}{2} (1-t^2) \right] G(\rho, \omega, q_{0C}, p', p, t) \right\}, \quad (74)$$

$$V_{10,10}(p', p) = 2\pi \int_{-1}^1 dt \left\{ \frac{gg'}{2f_\pi^2} \frac{1}{30} [4(p'^2 + p^2)t + p' p (-21 + 13t^2)] G(\pi, \eta, q_{0D}, p', p, t) \right\}$$

$$\begin{aligned}
& -\frac{f'^2}{2f_\pi^2}q_{0C}^2tG(\pi, \eta, q_{0C}, p', p, t) - g_\sigma g'_\sigma tG(m_\sigma, q_{0D}, p', p, t) \\
& -\frac{h_\sigma^2}{f_\pi^2}\frac{1}{30}\left[4(p'^2 + p^2)t + p'p(-21 + 13t^2)\right]G(m_\sigma, q_{0C}, p', p, t) \\
& + g_V^2\left[\frac{1}{4}\beta\beta_1t - \lambda\lambda_1\frac{1}{30}(34(p'^2 + p^2)t - p'p(21 + 47t^2))\right]G(\rho, \omega, q_{0D}, p', p, t) \\
& + g_V^2\left[\frac{1}{4}(\zeta - 2\mu q_{0C})^2t + \mu^2\frac{1}{30}(4(p'^2 + p^2)t + p'p(-21 + 13t^2))\right]G(\rho, \omega, q_{0C}, p', p, t) \Big\}, \quad (75)
\end{aligned}$$

$$V_{89}(p', p) = 0, \quad V_{9,10}(p', p) = 0,$$

$$\begin{aligned}
V_{8,10}(p', p) = 2\pi \int_{-1}^1 dt \Bigg\{ & -\frac{gg'}{2f_\pi^2}\frac{1}{3\sqrt{5}}\left[2(p'^2 + p^2)t - p'p(3 + t^2)\right]G(\pi, \eta, q_{0D}, p', p, t) \\
& + \frac{h_\sigma^2}{f_\pi^2}\frac{1}{3\sqrt{5}}\left[2(p'^2 + p^2)t - p'p(3 + t^2)\right]G(m_\sigma, q_{0C}, p', p, t) \\
& + g_V^2\lambda\lambda_1\frac{1}{3\sqrt{5}}\left[2(p'^2 + p^2)t - p'p(3 + t^2)\right]G(\rho, \omega, q_{0D}, p', p, t) \\
& - g_V^2\mu^2\frac{1}{3\sqrt{5}}\left[2(p'^2 + p^2)t - p'p(3 + t^2)\right]G(\rho, \omega, q_{0C}, p', p, t) \Bigg\}. \quad (76)
\end{aligned}$$

—————

The partial wave projected potentials for $D^*\bar{D}_1 \rightarrow D^*\bar{D}_1$ (channels 11–13) are:

$$\begin{aligned}
V_{11,11}(p', p) = 2\pi \int_{-1}^1 tdt \Bigg\{ & -\frac{1}{3}\frac{(h_1 + h_2)^2}{2\Lambda_\chi^2 f_\pi^2}(p'^2 + p^2 - 2p'pt)^2G(\pi, \eta, q_{0C}, p', p, t) + \frac{5}{6}\frac{gg''}{2f_\pi^2}\frac{2}{3}(p'^2 + p^2 - 2p'pt) \\
& \times G(\pi, \eta, q_{0D}, p', p, t) - g_\sigma g''_\sigma G(m_\sigma, q_{0D}, p', p, t) - \frac{h_\sigma'^2}{6f_\pi^2}\frac{2}{3}(p'^2 + p^2 - 2p'pt)G(m_\sigma, q_{0C}, p', p, t) \\
& + g_V^2\left[\frac{1}{4}\beta\beta_2 - \frac{1}{2}\lambda\lambda_2\frac{4}{3}(p'^2 + p^2 - 2p'pt)\right]G(\rho, \omega, q_{0D}, p', p, t) \\
& + \frac{1}{24}g_V^2\left[-2(\zeta_1 + \mu_1 q_{0C})^2 + \mu_1^2\frac{2}{3}(p'^2 + p^2 - 2p'pt)\right]G(\rho, \omega, q_{0C}, p', p, t) \Bigg\}, \quad (77)
\end{aligned}$$

$$\begin{aligned}
V_{12,12}(p', p) = 2\pi \int_{-1}^1 dt \Bigg\{ & \frac{3}{2}\frac{(h_1 + h_2)^2}{2\Lambda_\chi^2 f_\pi^2}\frac{1}{18}\left[-4(p'^4 + p^4)t - 2p'^2p^2t(7 + 5t^2) \right. \\
& \left. + (p'^3p + p'p^3)(3 + 13t^2)\right]G(\pi, \eta, q_{0C}, p', p, t) + \frac{5}{6}\frac{gg''}{2f_\pi^2}\frac{1}{2}p'p(1 - t^2)G(\pi, \eta, q_{0D}, p', p, t) \\
& - g_\sigma g''_\sigma tG(m_\sigma, q_{0D}, p', p, t) + \frac{h_\sigma'^2}{6f_\pi^2}\frac{1}{2}p'p(1 - t^2)G(m_\sigma, q_{0C}, p', p, t) \\
& + g_V^2\left[\frac{1}{4}\beta\beta_2t + \frac{1}{2}\lambda\lambda_2\left(-(p'^2 + p^2)t + p'p\frac{1}{2}(1 + 3t^2)\right)\right]G(\rho, \omega, q_{0D}, p', p, t) \\
& - \frac{1}{24}g_V^2\left[-(\zeta_1 + \mu_1 q_{0C})^2t + \mu_1^2\frac{1}{2}p'p(1 - t^2)\right]G(\rho, \omega, q_{0C}, p', p, t) \Bigg\}, \quad (78)
\end{aligned}$$

$$\begin{aligned}
V_{13,13}(p', p) = 2\pi \int_{-1}^1 dt \Bigg\{ & -\frac{3}{2}\frac{(h_1 + h_2)^2}{2\Lambda_\chi^2 f_\pi^2}\frac{1}{30}p'p(p'^2 + p^2 - 2p'pt)(1 - t^2)G(\pi, \eta, q_{0C}, p', p, t) \\
& + \frac{5}{6}\frac{gg''}{2f_\pi^2}\frac{1}{30}\left[4(p'^2 + p^2)t + p'p(-21 + 13t^2)\right]G(\pi, \eta, q_{0D}, p', p, t)
\end{aligned}$$

$$\begin{aligned}
& -g_\sigma g_\sigma'' t G(m_\sigma, q_{0D}, p', p, t) - \frac{h_\sigma'^2}{6f_\pi^2} \frac{1}{30} [4(p'^2 + p^2)t + p'p(-21 + 13t^2)] G(m_\sigma, q_{0C}, p', p, t) \\
& + g_V^2 \left[\frac{1}{4} \beta \beta_2 t + \frac{1}{2} \lambda \lambda_2 \frac{1}{30} (34(p'^2 + p^2)t - p'p(21 + 47t^2)) \right] G(\rho, \omega, q_{0D}, p', p, t) \\
& + \frac{1}{24} g_V^2 \left[(\zeta_1 + \mu_1 q_{0C})^2 t + \mu_1^2 \frac{1}{30} (4(p'^2 + p^2)t + p'p(-21 + 13t^2)) \right] G(\rho, \omega, q_{0C}, p', p, t) \Big\}, \tag{79}
\end{aligned}$$

$$V_{11,12}(p', p) = 0, \quad V_{12,13}(p', p) = 0,$$

$$\begin{aligned}
V_{11,13}(p', p) = & 2\pi \int_{-1}^1 dt \left\{ -\frac{3}{2} \frac{(h_1 + h_2)^2}{2\Lambda_\chi^2 f_\pi^2} \frac{1}{9\sqrt{5}} [2(p'^4 + p^4)t + 2p'^2 p^2 t(5 + t^2) - (p'^3 p + p' p^3)(3 + 5t^2)] G(\pi, \eta, q_{0C}, p', p, t) \right. \\
& - \frac{5}{6} \frac{gg''}{2f_\pi^2} \frac{1}{3\sqrt{5}} [2(p'^2 + p^2)t - p'p(3 + t^2)] G(\pi, \eta, q_{0D}, p', p, t) + \frac{h_\sigma'^2}{6f_\pi^2} \frac{1}{3\sqrt{5}} [2(p'^2 + p^2)t - p'p(3 + t^2)] \\
& \times G(m_\sigma, q_{0C}, p', p, t) - \frac{1}{2} g_V^2 \lambda \lambda_2 \frac{1}{3\sqrt{5}} [2(p'^2 + p^2)t - p'p(3 + t^2)] G(\rho, \omega, q_{0D}, p', p, t) \\
& \left. - \frac{1}{24} g_V^2 \mu_1^2 \frac{1}{3\sqrt{5}} [2(p'^2 + p^2)t - p'p(3 + t^2)] G(\rho, \omega, q_{0C}, p', p, t) \right\}. \tag{80}
\end{aligned}$$

The partial wave projected potentials for $D^* \bar{D}_2^* \rightarrow D^* \bar{D}_2^*$ (channels 14–15) are:

$$\begin{aligned}
V_{14,14}(p', p) = & 2\pi \int_{-1}^1 dt \left\{ -\frac{gg''}{2f_\pi^2} \frac{3}{20} [4(p'^2 + p^2)t - p'p(1 + 7t^2)] G(\pi, \eta, q_{0D}, p', p, t) \right. \\
& + \frac{(h_1 + h_2)^2}{2\Lambda_\chi^2 f_\pi^2} \frac{3}{20} p'p(p'^2 + p^2 - 2p'pt)(1 - t^2) G(\pi, \eta, q_{0C}, p', p, t) \\
& - g_\sigma g_\sigma'' t G(m_\sigma, q_{0D}, p', p, t) + \frac{h_\sigma'^2}{f_\pi^2} \frac{1}{60} [-12(p'^2 + p^2)t + p'p(23 + t^2)] G(m_\sigma, q_{0C}, p', p, t) \\
& + g_V^2 \left[\frac{1}{4} \beta \beta_2 t + \lambda \lambda_2 \frac{3}{20} [6(p'^2 + p^2)t + p'p(1 - 13t^2)] \right] G(\rho, \omega, q_{0D}, p', p, t) \\
& \left. + \frac{g_V^2}{4} \left[\frac{1}{6} (\zeta_1 - \mu_1 q_{0C})^2 t - \mu_1^2 \frac{1}{60} [-12(p'^2 + p^2)t + p'p(23 + t^2)] \right] G(\rho, \omega, q_{0C}, p', p, t) \right\}, \tag{81}
\end{aligned}$$

$$\begin{aligned}
V_{15,15}(p', p) = & 2\pi \int_{-1}^1 dt \left\{ \frac{gg''}{2f_\pi^2} \frac{1}{20} [-8(p'^2 + p^2)t + p'p(7 + 9t^2)] G(\pi, \eta, q_{0D}, p', p, t) \right. \\
& - \frac{(h_1 + h_2)^2}{2\Lambda_\chi^2 f_\pi^2} \frac{1}{20} [4(p'^4 + p^4)t + 2p'^2 p^2 t(5 + 7t^2) - (p'^3 p + p' p^3)(1 + 15t^2)] G(\pi, \eta, q_{0C}, p', p, t) \\
& - g_\sigma g_\sigma'' t G(m_\sigma, q_{0D}, p', p, t) - \frac{h_\sigma'^2}{f_\pi^2} \frac{1}{20} [8(p'^2 + p^2)t - p'p(7 + 9t^2)] G(m_\sigma, q_{0C}, p', p, t) \\
& + g_V^2 \left[\frac{1}{4} \beta \beta_2 t + \lambda \lambda_2 \frac{1}{20} [2(p'^2 + p^2)t + p'p(7 - 11t^2)] \right] G(\rho, \omega, q_{0D}, p', p, t) \\
& \left. - \frac{g_V^2}{4} \left[\frac{1}{2} (\zeta_1 - \mu_1 q_{0C})^2 t - \mu_1^2 \frac{1}{20} [8(p'^2 + p^2)t - p'p(7 + 9t^2)] \right] G(\rho, \omega, q_{0C}, p', p, t) \right\}, \tag{82}
\end{aligned}$$

$$V_{14,15}(p', p) = 2\pi \int_{-1}^1 dt \left\{ \frac{gg''}{2f_\pi^2} \frac{\sqrt{3}}{10} [-2(p'^2 + p^2)t + p'p(3 + t^2)] G(\pi, \eta, q_{0D}, p', p, t) \right.$$

$$\begin{aligned}
& + \frac{h_\sigma'^2}{f_\pi^2} \frac{1}{5\sqrt{3}} [2(p'^2 + p^2)t - p'p(3 + t^2)] G(m_\sigma, q_{0C}, p', p, t) \\
& + g_V^2 \left[\lambda \lambda_2 \frac{\sqrt{3}}{10} [-2(p'^2 + p^2)t + p'p(3 + t^2)] \right] G(\rho, \omega, q_{0D}, p', p, t) \\
& - \frac{g_V^2}{4} \left[\mu_1^2 \frac{1}{5\sqrt{3}} [2(p'^2 + p^2)t - p'p(3 + t^2)] \right] G(\rho, \omega, q_{0C}, p', p, t) \Big\}. \tag{83}
\end{aligned}$$

D. Appendix D: Decay widths of D_0^* , D_1' , D_1 , and D_2^*

In this appendix, we assume that the total widths of the unstable mesons D_0^* , D_1' , D_1 , and D_2^* are dominated by their two-body strong decays into the $D^{(*)}\pi$ channels. Given the large phase space available for these decays, isospin symmetry breaking effects are expected to be negligible. Consequently, based on isospin symmetry, the partial widths satisfy the relation $\Gamma(B \rightarrow D^{(*)}\pi^+) = 2\Gamma(B \rightarrow D^{(*)}\pi^0)$, where B denotes the initial unstable meson. The explicit formulas for the decay widths into the charged pion mode (π^+) are given by:

$$\Gamma(D_0^* \rightarrow D\pi^+) = \frac{f''}{2\pi f_\pi^2} \frac{m_D}{m_{D_0^*}} k_\pi E_\pi^2, \tag{84}$$

$$\Gamma(D_1' \rightarrow D^*\pi^+) = \frac{f''}{2\pi f_\pi^2} \frac{m_{D^*}}{m_{D_1'}} k_\pi E_\pi^2, \tag{85}$$

$$\Gamma(D_1 \rightarrow D^*\pi^+) = \frac{1}{6\pi f_\pi^2} \left(\frac{h_1 + h_2}{\Lambda_\chi} \right)^2 \frac{m_{D^*}}{m_{D_1}} k_\pi^5, \tag{86}$$

$$\Gamma(D_2^* \rightarrow D\pi^+) = \frac{1}{15\pi f_\pi^2} \left(\frac{h_1 + h_2}{\Lambda_\chi} \right)^2 \frac{m_D}{m_{D_2^*}} k_\pi^5, \tag{87}$$

$$\Gamma(D_2^* \rightarrow D^*\pi^+) = \frac{1}{10\pi f_\pi^2} \left(\frac{h_1 + h_2}{\Lambda_\chi} \right)^2 \frac{m_{D^*}}{m_{D_2^*}} k_\pi^5. \tag{88}$$

where k_π is the momentum of the pion in the rest frame of the decaying particle B , defined as:

$$\begin{aligned}
k_\pi &= \frac{1}{2E_{D_0^*}} \lambda^{1/2}(m_B^2, m_{D^{(*)}}^2, m_\pi^2), \\
\lambda(a, b, c) &= a^2 + b^2 + c^2 - 2ab - 2bc - 2ac. \tag{89}
\end{aligned}$$

Here, M_B represents the effective mass (or running energy \sqrt{s}) of the unstable particle B (e.g., $E_{D_0^*}$ as defined in Eq. (10)) when considering self-energy corrections.

- [1] S.-K. Choi *et al.* (Belle Collaboration), Observation of a Narrow Charmoniumlike State in Exclusive $B^\pm \rightarrow K^\pm \pi^+ \pi^- J/\psi$ Decays, *Phys. Rev. Lett.* **91**, 262001 (2003).
- [2] M. Ablikim *et al.* (BESIII Collaboration), Observation of a Charged Charmoniumlike Structure in $e^+e^- \rightarrow \pi^+ \pi^- J/\psi$ at $\sqrt{s} = 4.26$ GeV, *Phys. Rev. Lett.* **110**, 252001 (2013).
- [3] Z. Q. Liu *et al.* (Belle Collaboration), Study of $e^+e^- \rightarrow \pi^+ \pi^- J/\psi$ and Observation of a Charged Charmoniumlike State at Belle, *Phys. Rev. Lett.* **110**, 252002 (2013).
- [4] M. Ablikim *et al.* (BESIII Collaboration), Observation of a Charged Charmoniumlike Structure $Z_c(4020)$ and Search for the $Z_c(3900)$ in $e^+e^- \rightarrow \pi^+ \pi^- h_c$, *Phys. Rev. Lett.* **111**, 242001 (2013).
- [5] R. Aaij *et al.* (LHCb Collaboration), Observation of an exotic narrow doubly charmed tetraquark, *Nat. Phys.* **18**, 751 (2022).
- [6] R. Aaij *et al.* (LHCb Collaboration), Study of the doubly charmed tetraquark T_{cc}^+ , *Nat. Commun.* **13**, 3351 (2022).
- [7] A. Hosaka, T. Iijima, K. Miyabayashi, Y. Sakai, and S. Yasui, Exotic hadrons with heavy flavors: X, Y, Z, and related states, *Prog. Theor. Exp. Phys.* **2016**, 062C01 (2016).
- [8] H.-X. Chen, W. Chen, X. Liu, and S.-L. Zhu, The hidden-charm pentaquark and tetraquark states, *Phys. Rep.* **639**, 1 (2016).
- [9] H.-X. Chen, W. Chen, X. Liu, Y.-R. Liu, and S.-L. Zhu, A review of the open charm and open bottom systems, *Rep. Prog. Phys.* **80**, 076201 (2017).
- [10] A. Ali, J. S. Lange, and S. Stone, Exotics: Heavy Pentaquarks and Tetraquarks, *Prog. Part. Nucl. Phys.* **97**, 123 (2017).
- [11] A. Esposito, A. Pilloni, and A. D. Polosa, Multiquark resonances, *Phys. Rep.* **668**, 1 (2017).
- [12] R. F. Lebed, R. E. Mitchell, and E. S. Swanson, Heavy-Quark QCD Exotica, *Prog. Part. Nucl. Phys.* **93**, 143 (2017).
- [13] F.-K. Guo, C. Hanhart, U.-G. Meißner, Q. Wang, Q. Zhao, and B.-S. Zou, Hadronic molecules, *Rev. Mod. Phys.* **90**, 015004 (2018).
- [14] Y.-R. Liu, H.-X. Chen, W. Chen, X. Liu, and S.-L. Zhu, Pentaquark and tetraquark states, *Prog. Part. Nucl. Phys.* **107**, 237 (2019).
- [15] N. Brambilla *et al.*, The XYZ states: Experimental and theoretical status and perspectives, *Phys. Rep.* **873**, 1 (2020).
- [16] W. Lucha, D. Melikhov, and H. Sazdjian, Tetraquarks in large- N_c QCD, *Prog. Part. Nucl. Phys.* **120**, 103867 (2021).
- [17] X.-K. Dong, F.-K. Guo, and B.-S. Zou, A survey of heavy-heavy hadronic molecules, *Commun. Theor. Phys.* **73**, 125201 (2021).

[18] N. Brambilla, S. Eidelman, C. Hanhart, A. Nefediev, C.-P. Shen, C. E. Thomas, A. Vairo, and C.-Z. Yuan, Effective Field Theories and Lattice QCD for the X Y Z frontier, *PoS LATTICE2021*, 020 (2022).

[19] L. Meng, B. Wang, G.-J. Wang, and S.-L. Zhu, Chiral perturbation theory for heavy hadrons and chiral effective field theory for heavy hadronic molecules, *Phys. Rep.* **1019**, 1 (2023).

[20] H.-X. Chen, W. Chen, X. Liu, Y.-R. Liu, and S.-L. Zhu, An updated review of the new hadron states, *Rep. Prog. Phys.* **86**, 026201 (2023).

[21] R. Molina and E. Oset, $Y(3940)$, $Z(3930)$, and the $X(4160)$ as dynamically generated resonances from the vector-vector interaction, *Phys. Rev. D* **80**, 114013 (2009).

[22] J.-R. Zhang, M. Zhong, and M.-Q. Huang, Could $Z_b(10610)$ be a $B^* \bar{B}$ molecular state?, *Phys. Lett. B* **704**, 312 (2011).

[23] Z.-F. Sun, J. He, X. Liu, Z.-G. Luo, and S.-L. Zhu, $Z_b(10610)^\pm$ and $Z_b(10650)^\pm$ as the $B^* B$ and $B^* B^*$ molecular states, *Phys. Rev. D* **84**, 054002 (2011).

[24] A. Ozpineci, C. W. Xiao, and E. Oset, Hidden beauty molecules within the local hidden gauge approach and heavy quark spin symmetry, *Phys. Rev. D* **88**, 034018 (2013).

[25] J. He, X. Liu, Z.-F. Sun, and S.-L. Zhu, $z_c(4025)$ as the hadronic molecule with hidden charm, *Eur. Phys. J. C* **73**, 2635 (2013).

[26] F.-K. Guo, C. Hidalgo-Duque, J. Nieves, and M. P. Valderrama, Consequences of heavy-quark symmetries for hadronic molecules, *Phys. Rev. D* **88**, 054007 (2013).

[27] Y. Dong, A. Faessler, T. Gutsche, and V. E. Lyubovitskij, Strong decays of molecular states Z_c^+ and $Z_c'^+$, *Phys. Rev. D* **88**, 014030 (2013).

[28] Z.-G. Wang and T. Huang, Possible assignments of the $X(3872)$, $Z_c(3900)$, and $Z_b(10610)$ as axial-vector molecular states, *Eur. Phys. J. C* **74**, 2891 (2014).

[29] J. He, Study of $B\bar{B}^*/D\bar{D}^*$ bound states in a Bethe-Salpeter approach, *Phys. Rev. D* **90**, 076008 (2014).

[30] F. Aceti, M. Bayar, E. Oset, A. M. Torres, K. P. Khemchandani, J. M. Dias, F. S. Navarra, and M. Nielsen, Prediction of an $I = 1$ $D\bar{D}^*$ state and relationship to the claimed $Z_c(3900)$, $Z_c(3885)$, *Phys. Rev. D* **90**, 016003 (2014).

[31] Z.-G. Wang, Reanalysis of the $Y(3940)$, $Y(4140)$, $Z_c(4020)$, $Z_c(4025)$, and $Z_b(10650)$ as molecular states with QCD sum rules, *Eur. Phys. J. C* **74**, 2963 (2014).

[32] M. Karliner and J. L. Rosner, New Exotic Meson and Baryon Resonances from Doubly Heavy Hadronic Molecules, *Phys. Rev. Lett.* **115**, 122001 (2015).

[33] V. Baru, A. A. Filin, C. Hanhart, A. V. Nefediev, Q. Wang, and J.-L. Wynen, Properties of $Z_b(10610)$ and $Z_b(10650)$ from an Analysis of Experimental Line Shapes, *EPJ Web Conf.* **202**, 06012 (2019).

[34] B. Wang, L. Meng, and S.-L. Zhu, Deciphering the charged heavy quarkoniumlike states in chiral effective field theory, *Phys. Rev. D* **102**, 114019 (2020).

[35] Z.-M. Ding, H.-Y. Jiang, and J. He, Molecular states from $D^{(*)}\bar{D}^{(*)}/B^{(*)}\bar{B}^{(*)}$ and $D^{(*)}D^{(*)}/\bar{B}^{(*)}\bar{B}^{(*)}$ interactions, *Eur. Phys. J. C* **80**, 1179 (2020).

[36] L. R. Dai, E. Oset, A. Feijoo, R. Molina, L. Roca, A. M. Torres, and K. P. Khemchandani, Masses and widths of the exotic molecular $B_{(s)}^{(*)}B_{(s)}^{(*)}$ states, *Phys. Rev. D* **105**, 074017 (2022).

[37] R. Aaij *et al.* (LHCb Collaboration), Observation and Investigation of the $T_{c\bar{c}1}(4430)^+$ Structure in $B^+ \rightarrow \psi(2S)K_S^0\pi^+$ Decays, (2025), arXiv:2511.20428 [hep-ex].

[38] S.-K. Choi *et al.* (Belle Collaboration), Observation of a Resonance-like Structure in the $\pi^\pm\psi'$ Mass Distribution in Exclusive $B \rightarrow K\pi^\pm\psi'$ Decays, *Phys. Rev. Lett.* **100**, 142001 (2008).

[39] R. Aaij *et al.* (LHCb Collaboration), Observation of the Resonant Character of the $Z(4430)^-$ State, *Phys. Rev. Lett.* **112**, 222002 (2014).

[40] X. Liu, Y.-R. Liu, W.-Z. Deng, and S.-L. Zhu, $Z^+(4430)$ as a $D'_1 D^*$ ($D_1 D^*$) molecular state, *Phys. Rev. D* **77**, 094015 (2008).

[41] X. Liu, Y.-R. Liu, W.-Z. Deng, and S.-L. Zhu, Is $Z^+(4430)$ a loosely bound molecular state?, *Phys. Rev. D* **77**, 034003 (2008).

[42] J. He and P.-L. Lü, $D^*\bar{D}_1(2420)$ and $D\bar{D}^*(2600)$ interactions and the charged charmonium-like state $Z(4430)$, *Chin. Phys. C* **40**, 043101 (2016).

[43] J. He and D.-Y. Chen, Interpretation of $Y(4390)$ as an Isoscalar Partner of $Z(4430)$ from $D^*(2010)\bar{D}_1(2420)$ Interaction, *Eur. Phys. J. C* **77**, 4973 (2017).

[44] L. Ma, X.-H. Liu, X. Liu, and S.-L. Zhu, Exotic four quark matter: $Z_1(4475)$, *Phys. Rev. D* **90**, 037502 (2014).

[45] X.-H. Liu, L. Ma, L.-P. Sun, X. Liu, and S.-L. Zhu, Resolving the puzzling decay patterns of charged Z_c and Z_b states, *Phys. Rev. D* **90**, 074020 (2014).

[46] X.-H. Liu, Q. Zhao, and F. E. Close, Search for tetraquark candidate $Z(4430)$ in meson photoproduction, *Phys. Rev. D* **77**, 094005 (2008).

[47] A. L. Guerrieri, F. Piccinini, A. Pilloni, and A. D. Polosa, Production of tetraquarks at the LHC, *Phys. Rev. D* **90**, 034003 (2014).

[48] L. Maiani, A. D. Polosa, and V. Riquer, The Charged $Z(4430)$ in the Diquark-Antidiquark Picture, *New J. Phys.* **10**, 073004 (2008).

[49] D. Ebert, R. N. Faustov, and V. O. Galkin, Excited heavy tetraquarks with hidden charm, *Eur. Phys. J. C* **58**, 399 (2008).

[50] M. E. Bracco, S. H. Lee, M. Nielsen, and R. R. D. Silva, The Meson $Z^+(4430)$ as a Tetraquark State, *Phys. Lett. B* **671**, 240 (2009).

[51] Z.-G. Wang, Mass spectrum of the axial-vector hidden charmed and hidden bottom tetraquark states, *Eur. Phys. J. C* **70**, 139 (2010).

[52] L. Maiani, F. Piccinini, A. D. Polosa, and V. Riquer, $Z(4430)$ and a new paradigm for spin interactions in tetraquarks, *Phys. Rev. D* **89**, 114010 (2014).

[53] C. Deng, J. Ping, H. Huang, and F. Wang, Systematic study of Z_c^+ family from a multiquark color flux-tube model, *Phys. Rev. D* **92**, 034027 (2015).

[54] Z.-G. Wang, Analysis of the $Z(4430)$ as the First Radial Excitation of the $Z_c(3900)$, *Commun. Theor. Phys.* **63**, 325 (2015).

[55] S. S. Agaev, K. Azizi, and H. Sundu, Treating $Z_c(3900)$ and $Z(4430)$ as the ground state and first radially excited tetraquarks, *Phys. Rev. D* **96**, 034026 (2017).

[56] K. Azizi and N. Er, Modifications on Parameters of $Z(4430)$ in a Dense Medium, *Phys. Lett. B* **811**, 135979 (2020).

[57] S. X. Nakamura, $Z_c(4430)$, $Z_c(4200)$, $Z_1(4050)$, and $Z_2(4250)$ as Triangle Singularities, *AIP Conf. Proc.* **2249**, 030006 (2020).

[58] F.-K. Guo, X.-H. Liu, and S. Sakai, Threshold cusps and triangle singularities in hadronic reactions, *Prog. Part. Nucl. Phys.* **112**, 103757 (2020).

[59] J. L. Rosner, Threshold effect and $\pi^\pm\psi(2S)$ peak, *Phys. Rev. D* **76**, 114002 (2007).

[60] J.-B. Cheng, Z.-Y. Lin, and S.-L. Zhu, Double-charm tetraquark under the complex scaling method, *Phys. Rev. D* **106**, 016012 (2022).

[61] Z.-Y. Lin, J.-B. Cheng, and S.-L. Zhu, T_{cc}^+ and $\chi_{c1}(3872)$ with the complex scaling method and $DD(\bar{D})\pi$ three-body effect, *Phys. Rev. D* **110**, 054008 (2024).

[62] Z.-Y. Lin, J.-Z. Wang, J.-B. Cheng, L. Meng, and S.-L. Zhu, Identification of the $G(3900)$ Structure as the P -Wave $D\bar{D}^*/\bar{D}D^*$ Resonance, *Phys. Rev. Lett.* **133**, 241903 (2024).

[63] S. Navas *et al.* (Particle Data Group), Review of particle physics, *Phys. Rev. D* **110**, 030001 (2024).

[64] J. Aguilar and J. M. Combes, A class of analytic perturbations for one-body Schrödinger Hamiltonians, *Commun. Math. Phys.* **22**, 269 (1971).

[65] E. Balslev and J. M. Combes, Spectral properties of many-body Schrödinger operators with dilatation-analytic interactions, *Commun. Math. Phys.* **22**, 280 (1971).

[66] Y.-K. Chen, L. Meng, Z.-Y. Lin, and S.-L. Zhu, Virtual states in the coupled-channel problems with an improved complex scaling method, *Phys. Rev. D* **109**, 034006 (2024).

[67] Z.-Y. Lin, J.-B. Cheng, B.-L. Huang, and S.-L. Zhu, Partial widths from analytical extension of the wave function: P_c states, *Phys. Rev. D* **108**, 114014 (2023).

[68] J.-B. Cheng, B.-L. Huang, Z.-Y. Lin, and S.-L. Zhu, Z_c , Z_c and Z_b states under the complex scaling method, *Eur. Phys. J. C* **83**, 1071 (2023).

[69] H.-X. Zhu, L. Meng, Y. Ma, N. Li, W. Chen, and S.-L. Zhu, Constraining the $D\bar{D}D^*$ three-body bound state via the $Z_c(3900)$ pole, *Phys. Rev. D* **111**, 094022 (2025).

[70] J.-Z. Wang, Z.-Y. Lin, B. Wang, L. Meng, and S.-L. Zhu, Double pole structures of $X_1(2900)$ as the P -wave \bar{D}^*K^* resonances, *Phys. Rev. D* **110**, 114003 (2024).

[71] J.-Z. Wang, Z.-Y. Lin, and S.-L. Zhu, Cut Structures and an Observable Singularity in the Three-Body Threshold Dynamics: The T_{cc}^+ Case, *Phys. Rev. D* **109**, L071505 (2024).

[72] H. Masui, S. Aoyama, T. Myo, and K. Kato, Partial Decay Widths in Coupled-Channel Systems with the Complex-Scaled Jost Function Method, *Prog. Theor. Phys.* **102**, 1119 (1999).

[73] A. V. Manohar and M. B. Wise, *Heavy Quark Physics* (Cambridge University Press, Cambridge ; New York, 2000).

[74] A. Manohar and H. Georgi, Chiral Quarks and the Non-relativistic Quark Model, *Nucl. Phys. B* **234**, 189 (1984).

[75] Q.-T. Song, D.-Y. Chen, X. Liu, and T. Matsuki, Higher radial and orbital excitations in the charmed meson family, *Phys. Rev. D* **92**, 074011 (2015).

[76] S. Ahmed *et al.* (CLEO Collaboration), First Measurement of $\Gamma(D^{*+})$, *Phys. Rev. Lett.* **87**, 251801 (2001).

[77] M. Bando, T. Kugo, and K. Yamawaki, Nonlinear realization and hidden local symmetries, *Phys. Rep.* **164**, 217 (1988).

[78] C. Isola, M. Ladisa, G. Nardulli, and P. Santorelli, Charming penguin contributions in $B \rightarrow K^*\pi, K(\rho, \omega, \phi)$ decays, *Phys. Rev. D* **68**, 114001 (2003).

[79] U. Vogl and W. Weise, The Nambu and Jona Lasinio model: Its implications for hadrons and nuclei, *Prog. Part. Nucl. Phys.* **27**, 195 (1991).